12-2018

A Structural and Stratigraphic Study of the A-2 Carbonate in Southwest Michigan and Reservoir Characterization of an A-2 Carbonate Gas Storage Field

Clayton Joupperi

A STRUCTURAL AND STRATIGRAPHIC STUDY OF THE A-2 CARBONATE IN SOUTHWEST MICHIGAN AND RESERVOIR CHARACTERIZATION OF AN A-2 CARBONATE GAS STORAGE FIELD

by

Clayton Daniel Joupperi

A thesis submitted to the Graduate College
in partial fulfillment of the requirements
for the degree of Master of Science
Geological and Environmental Sciences
Western Michigan University
December 2018

Thesis Committee:

Donald M. Reeves, Ph.D., Chair
William Harrison III, Ph.D.
Peter Voice, Ph.D.

ACKNOWLEDGEMENTS

I would like to acknowledge the people who have helped me along the way during my time at Western Michigan University. My advisor, Matt Reeves for his willingness to take me on as his student and for giving me every opportunity to succeed. My committee members, Bill Harrison and Peter Voice for providing their insightful comments and providing me with abundant resources. Thank you to Linda Harrison and Jenny Trout for welcoming me at MGRRE and making it a second home for me. To the Department of Geological and Environmental Sciences for a graduate assistantship position. To Rob Chapman for taking interest in my project and helping immensely. I would like to thank my girlfriend, Julie Muldowney, for her support and patience while I pursue my goals. And to my mother, Carrie Joupperi, who has always supported me in all facets of life. Thank you all for the support.

Clayton D. Joupperi

A STRUCTURAL AND STRATIGRAPHIC STUDY OF THE A-2 CARBONATE IN SOUTHWEST MICHIGAN AND RESERVOIR CHARACTERIZATION OF AN A-2 CARBONATE GAS STORAGE FIELD

Clayton Daniel Joupperi, M.S.

Western Michigan University, 2018

The Overisel and Salem gas storage fields of southwest Michigan annually store 34 Bcf of natural working gas in the upper dolomitized portion of the Silurian A-2 Carbonate. Porosity and permeability in these fields is thought to be enhanced by fracturing and dolomitization associated with the dissolution and collapse of underlying salt units. This study utilizes wire-line logs from 383 wells to explore the structural and stratigraphic controls on the deposition and diagenesis of the A-2 Carbonate in southwest Michigan. Core and thin sections from 4 wells serve as the primary data for investigating the depositional and diagenetic history of the A-2 Carbonate. A three-dimensional static reservoir model of the Overisel field is generated from petrophysical porosity and permeability values from 77 wells. Production and well test data are used to investigate larger scale permeability trends and the potential role that fractures may have on the Overisel reservoir. Structure of the A-2 Carbonate fields in southwest Michigan is likely controlled by a combination of basement features and dissolution of the underlying A-1 Evaporite. Facies analysis of core and thin sections suggest that the A-2 Carbonate was deposited in an arid tidal flat, sabkha environment with diagenesis varying on a regional scale. The 3D static reservoir model indicates three zones in the structurally higher parts of the Overisel reservoir with favorably higher permeability and porosity. Estimated permeability from transient gas flow well tests are, on average, five times greater than core permeability values suggesting that fractures contribute to enhanced permeability in the Overisel reservoir. Analysis of the production and well test data indicate that the structurally higher sections of the A-2 Carbonate are the most productive, and acidizing and hydraulic fracturing of the A-2 Carbonate are key components of reservoir production.

TABLE OF CONTENTS

Table of Contents - Continued

LIST OF TABLES

LIST OF FIGURES

CHAPTER I

INTRODUCTION

Michigan is the 20th largest producer of oil and the 18th largest producer of natural gas in the United States (U.S. Energy Information Administration, 2016). The Salina A-2 Carbonate is generally overlooked as a profitable play in Michigan when compared to the underlying Guelph Dolomite (also known as "Brown Niagaran") reef plays. However, over 1 million barrels of oil and close to 63.3 billion cubic feet (Bcf) of gas have been produced from A-2 Carbonate reservoirs in southern Michigan. Almost all the gas producing fields were discovered before the 1960s and much of the data associated with the fields are dated, unreliable, or inaccessible. New analysis and synthesis of available data on the A-2 Carbonate can advance our knowledge and possibly stimulate exploration for new A-2 Carbonate gas fields. The Overisel and Salem fields in southwest Michigan are two of the most productive natural gas fields hosted in the A-2 Carbonate and are the focus of this study.

Efficient operation of these reservoirs is critical for maximizing natural gas storage and withdrawals and minimizing gas loss. Gas production and storage for the Overisel and Salem fields occurs in dolomitic units of the A-2 Carbonate that are believed to have enhanced porosity and permeability due to local fracturing. However, there has not been any fracture characterization studies of the A-2 Carbonate to determine if the fractures are sufficiently connected to form distinct networks that act as preferential fluid conduits. Studying cores of the A-2 Carbonate, along with the stratigraphy of underlying and overlying formations on a regional scale, can offer insight into the depositional and diagenetic history and distributions of the A-2 Carbonate and is useful for developing a conceptual geologic model for the field of interest. The conceptual geologic model can be paired with petrophysical data to generate a 3D static reservoir

model which can then be compared to production and well test data for identification of regions within the Overisel reservoir favorable for gas production and storage.

Subsurface Mapping using Wire-line Logs

Wire-line logs are used to identify and correlate the stratigraphic and structural relationships of unique rock formations and lithologies (Asquith and Krygowski, 2004). Gamma-ray logs measure the amount of radiation emitted by radioactive elements in rocks (primarily K, Th, and U). For example, distinct signatures differentiate carbonate lithofacies from anhydrite lithofacies caused by the relatively higher concentration of radioactive elements in the carbonate sediments. Neutron logs measure the hydrogen index of a formation by bombarding the rock with a radioactive neutron source. Neutron and hydrogen molecules are roughly the same size, and when the molecules collide a significant amount of energy is lost and not reflected back to the source. Anhydrite lacks hydrogen, and when bombarded with neutron molecules, relatively high neutron counts are measured since most neutron molecules are reflected back to the source. The high signatures of the anhydrite lithologies can easily be distinguished from carbonate sediment using neutron logs.

Distinguishing the top of geological formations is useful for understanding the stratigraphic and structural relationship of the rocks of interest and critical for geological visualization and interpretation. Structural investigations rely on these data to map the topography and thickness distributions of a rock formations and to identify productive reservoir zones and potential structural traps for hydrocarbons. Geologic cross-sections are useful for understanding stratigraphic relationships between different formations. Further analysis of

structural and stratigraphic relationships can then be used to understand how different rock formations were deposited and diagenetically altered in relation to one another.

Core and Thin Section Observations

Rock cores from wells have long been used to describe and analyze rocks in the subsurface. The scheme used by Dunham (1962) classifies carbonate rocks based on the abundance of framework grains and the mud matrix. Cores can be further examined using hand lens to identify sedimentary structures, pore types, and diagenetic features including fractures, dissolution, oil staining, and salt plugging. The lithology of carbonate rocks can further be investigated using hydrochloric acid because of the volatile reaction with limestone ($CaCO_3$) and weaker reaction with dolomite ($CaMg(CO_3)_2$).

Thin sections made from rock cores are examined using light microscopy to identify features on a much finer scale. Similar to observations made in core, crystal sizes, mineralogy, and textures along with diagenetic features including fractures, dissolution, and salt plugging can be observed in thin sections. Observations made from thin sections are often used to help characterize and better understand the rock composition observed in core. Core and thin section observations and analysis are useful for interpreting the depositional environment and diagenesis of rocks to enhance predictions of reservoir quality within a formation. By observing and comparing cores and thin sections from well to well, correlations can be made, and a depositional and diagenetic model can be interpreted.

Petrophysical Data from Core Analysis

Geologic interpretations of petroleum reservoirs and the inference of subsurface flow systems naturally exhibit a considerable amount of uncertainty. Uncertainty is a result of the generalization of micro-scale data from macro-scale observations and upscaling of the level of detail to a manageable size (Pettersen, 2006). For example, porosity and permeability values can vary considerably on a scale of meters. Porosity is a measurement of void space within a rock. Permeability and porosity are interrelated as permeability describes the ease of which a fluid can move through connected void spaces. Porosity and permeability are two of the most important petrophysical measurements for characterizing fluid pathways within a reservoir. These measurements are representative over small volumes defined by cores or flow rate tests, and it is often necessary to interpolate these known values over a formation or reservoir of interest. Although complex geological systems have irreducible uncertainty, petrophysical modeling is a critical step in characterizing productive regions within reservoir rock and formulating exploitation strategies. Analysis and interpretation of petrophysical data leads to greater understanding of the extent and magnitude of distinct porosity and permeability compartments in a reservoir.

Three-Dimensional Reservoir Modeling

Three-dimensional reservoir modeling is used for many purposes in the oil and gas industry today. Models are used for visualization of the reservoir architecture and internal stratigraphic relationships, all of which help to understand possible reservoir exploitation scenarios without the costs of real life trial and error (Pettersen, 2006). Construction of models is possible by distributing various rock properties and parameters into compartments of a 3D space

within a geological model template. A static reservoir model is used to describe the initial state of the reservoir prior to hydrocarbon production and represents the configuration and spatial distribution of rock types on the basis of reservoir properties (Rivenaes, 2015).

Prior to generation of a static 3D reservoir model, all relevant data and interpretations are used to form a conceptual geologic model (CGM). This includes data form wire-line logs, core and thin sections, engineering data, and the conceptual geological knowledge of the reservoir and area of interest (Pyrce, 2014). The CGM serves as the basis for inclusion of petrophysical data and ultimately, 3D static reservoir model generation. It is common for some wells and portions of the reservoir to have more complete data than others, and stochastic techniques are often needed to address variability between wells (Rivenaes, 2015) In these cases, conceptual geologic and structural knowledge must be utilized for prediction of modeled parameters within the more probabilistic, inter-well areas of the reservoir, and data gathered from wells serve as the foundation for the statistical and geospatial algorithms. If a large amount of petrophysical data is available before distribution throughout the CGM, the 3D static reservoir model will likely serve as a clear representation of the real-life reservoir.

Production and Well Test Data

The analysis of production and well test data helps to establish a baseline and identify more productive reservoir regions before and after the execution of well simulation techniques. Comparison of initial and post hydraulic fracturing/acidification production can provide additional insight into the spatial correlation of permeability within a reservoir. For example, acidizing and hydraulic sand fracturing can connect faults and fractures that were once completely isolated, changing reservoir function and performances near the well. Visualization

of interpolated pre- and post-stimulation production provides another level of reservoir characterization beyond a 3D static reservoir model populated with petrophysical data.

Gas well deliverability data such as computed averages of test flow rates and absolute open hole flow (AOF) can be used to determine the relative contributions of individual wells to overall gas flow and production. Test flow rates are collected during multi-point open-flow potential tests (OFPT) where a valve within the well is held at a constant opening, and flow rates are measured until the bottomhole pressure is stabilized. This indicates how an individual well performs at natural reservoir pressure. The AOF is calculated from isochronal well tests and measures the maximum well gas production volume at either the lowest possible bottom hole pressure or atmospheric pressure (SPE, 2015).

The average formation permeability for a section of rock surrounding a well can also be estimated from OFTP flowing bottom-hole pressure and flow rate data, where a linear relationship between the flow rates and pressures is used to compute the formation permeability thickness product (Matthews and Russell, 1967). Permeability estimates from well testing are extremely valuable as they represent in-situ measurements that sample significantly larger volumes of rock than cores. Comparisons between permeability estimates from core and well testing data allow for the interpretations of reservoir permeability at two separate scales.

Project Objectives

The objective of this project is to determine the stratigraphic and structural controls on deposition and diagenesis of the A-2 Carbonate in southwest Michigan, with a focus on the reservoir characterization of the Overisel gas storage field. This objective is addressed by investigating the following research questions:

1. What are the stratigraphic and geographic distributions of the Middle Silurian formations in southwest Michigan, and how do these formations contribute to the structural and stratigraphic controls on the A-2 Carbonate?
2. How can a depositional and diagenetic model for the A-2 Carbonate in southwest Michigan be developed from subsurface mapping and core observations?
3. How can a 3D static reservoir model be paired with production and well test data to identify regions within the Overisel field with favorable permeability and porosity values?

CHAPTER II

RESERVOIR CHARACTERIZATION AND 3D STATIC RESERVOIR MODELING OF A DOLOMITIZED A-2 CARBONATE GAS STORAGE RESERVOIR

The principal results of this research are presented as follows in the form of a manuscript to be submitted to the Society of Petroleum Engineers (SPE) Journal for publication. The SPE Journal is a bimonthly technical journal that is recognized in the industry as a leading peer-reviewed publication for information on new technologies and emerging concepts spanning all aspects of engineering for oil and gas exploration and production. The manuscript has been modified for this document and by providing reference to additional information (core photos, figures, and data) contained in Appendices that will not be included in the final manuscript.

The research manuscript is titled: *Reservoir Characterization and 3D Static Reservoir Modeling of a Dolomitized A-2 Carbonate Gas Storage Reservoir*. The study utilizes geological data such as wire-line logs, core, thin sections, core analysis and gas well deliverability data to characterize and model a gas storage reservoir in southwest Michigan. The model is intended to distinguish compartments of higher porosity and permeability within the gas storage reservoir and to detect preferential fluid pathways when compared to production and well test data. Study methodology, and results, and findings are thoroughly covered in the manuscript.

RESERVOIR CHARACTERIZATION AND 3D STATIC RESERVOIR MODELING OF A DOLOMITIZED A-2 CARBONATE GAS STORAGE RESERVOIR

Clay D. Joupperi, Donald M. Reeves*, William B. Harrison III and Peter J. Voice
Department of Geological and Environmental Sciences, Western Michigan University, Kalamazoo, MI 49008-5241 USA

*Corresponding author: matt.reeves@wmich.edu, Tel: (269)-387-5493

Abstract

The Overisel and Salem gas storage fields of southwest Michigan annually store 34 Bcf of natural working gas in the upper dolomitized portion of the Silurian A-2 Carbonate. Porosity and permeability in these fields is thought to be enhanced by fracturing and dolomitization associated with the dissolution and collapse of underlying salt units. This study utilizes wire-line logs from 383 wells to explore the structural and stratigraphic controls on the deposition and diagenesis of the A-2 Carbonate in southwest Michigan. Core and thin sections from 4 wells serve as the primary data for investigating the depositional and diagenetic history of the A-2 Carbonate. A three-dimensional static reservoir model of the Overisel field is generated from petrophysical porosity and permeability values from 77 wells. Production and well test data are used to investigate larger scale permeability trends and the potential role that fractures may have on the Overisel reservoir. Structure of the A-2 Carbonate fields in southwest Michigan is likely controlled by a combination of basement features and dissolution of the underlying A-1 Evaporite. Facies analysis of core and thin sections suggest that the A-2 Carbonate was deposited in an arid tidal flat, sabkha environment with diagenesis varying on a regional scale. The 3D static reservoir model indicates three zones in the structurally higher parts of the Overisel reservoir with favorably higher permeability and porosity. Estimated permeability from transient gas flow well tests are, on average, five times greater than core permeability values suggesting that fractures contribute to enhanced permeability in the Overisel reservoir. Analysis of the production and well test data indicate that the structurally higher sections of the A-2 Carbonate are the most productive, and acidizing and hydraulic fracturing of the A-2 Carbonate are key components of reservoir production.

Introduction

The Michigan Basin consists of mostly marine sedimentary rocks that range in age from Pre-Cambrian to Pennsylvanian, with a small portion of Jurassic rocks and glacial deposits overlying the Paleozoic rock record. Silurian aged rocks are present throughout most of the basin and account for 30 percent of the estimated total sediment (Cohee, 1965; Catocosinos, et al., 1990). Silurian rocks are particularly important from an economic perspective with over 500 million barrels of oil and 2.9 trillion cubic feet of natural gas having been produced from Silurian reservoirs. Of these totals, approximately 1 million barrels of oil and 63 billion cubic feet (Bcf) of gas has been produced from A-2 Carbonate reservoirs in southwest Michigan (State of Michigan, 2018b). Most of the structural and stratigraphic traps for these reservoirs are associated with the presence or absence of numerous evaporite formations. The A-2 Carbonate has historically been less studied than the other Silurian formations; however, regions of high reservoir quality in the A-2 Carbonate are generally attributed to dense fracturing (Ells, 1967).

Natural gas was first discovered in the Salem field in 1937 and in the Overisel field in 1956 (Ells, 1958), both of which are located along the southwest margin of the Michigan Basin in northern Allegan County (Figure 1). The dolomitic A-2 Carbonate unit serves as the primary gas storage reservoir in the Overisel and Salem fields. The Salem Field produced in excess of 11.5 Bcf of natural gas prior to gas storage reservoir in 1963 (State of Michigan, 2018b). In a span of four years the Overisel field produced nearly 15 Bcf of natural gas before being converted into a gas storage reservoir in 1960. Current estimates provided by Consumers Energy power company document that the total storage capacity for the Overisel and Salem fields are 53 and 30.5 Bcf of natural gas, with working gas volumes necessary to maintain reservoir pressures of 30 and 18.9 Bcf, respectively. This corresponds to 23 and 11.6 Bcf of natural gas available for

extraction and working gas to base ratios 38% to 43%. Efficient operation of these reservoirs requires detailed study of the Silurian stratigraphy within the Michigan Basin and petrophysical properties of the A-2 Carbonate. This requires better structural characterization of the A-2 Carbonate and more comprehensive analyses of reservoir permeability and variability and potential preferential fluid pathways that govern the storage and conveyance of natural gas.

The Michigan Basin is an intracratonic basin centered in the Lower Peninsula of Michigan and extends to parts of Ohio, Indiana, Illinois, and Wisconsin, as well as southwest Ontario, Canada (Figure 1(a)). It covers an area of 80,000 mi^2 that is defined by the Kankakee Arch to the southwest, the Wisconsin Arch to the west, the Algonquin Arch to the east, and the Canadian Shield to the north, with the deepest part of the basin located slightly east of the center of the Lower Peninsula (Catacosinos et al., 1990). Subsidence started during the Precambrian and reached maximum rates during the Late Silurian to Middle Devonian (Howell and van der Pluijm, 1999). Throughout the late Silurian, Michigan was a partially restricted basin as evidenced by reef belts that started forming in the middle Silurian, Homerian time (Cramer et al., 2011). In sub-tropical latitudes from 20 to 25 degrees south during subsequent Salina deposition (Scotese and McKerrow, 1990), Michigan experienced cyclic intervals of transgression and regression that led to the deposition of alternating evaporites and carbonates in the interior basin. Intervals of sea-level rise and fall are correlated to the deposition of the Salina Group formations (Figure 2). The Salina A-1 Evaporite, Salina A-2 Evaporite, and Salina B-Unit formations were deposited during intervals of lower sea-level, while intervals of higher sea-level led to the deposition of the Brown Niagaran, Salina A-1 Carbonate, and Salina A-2 Carbonate.

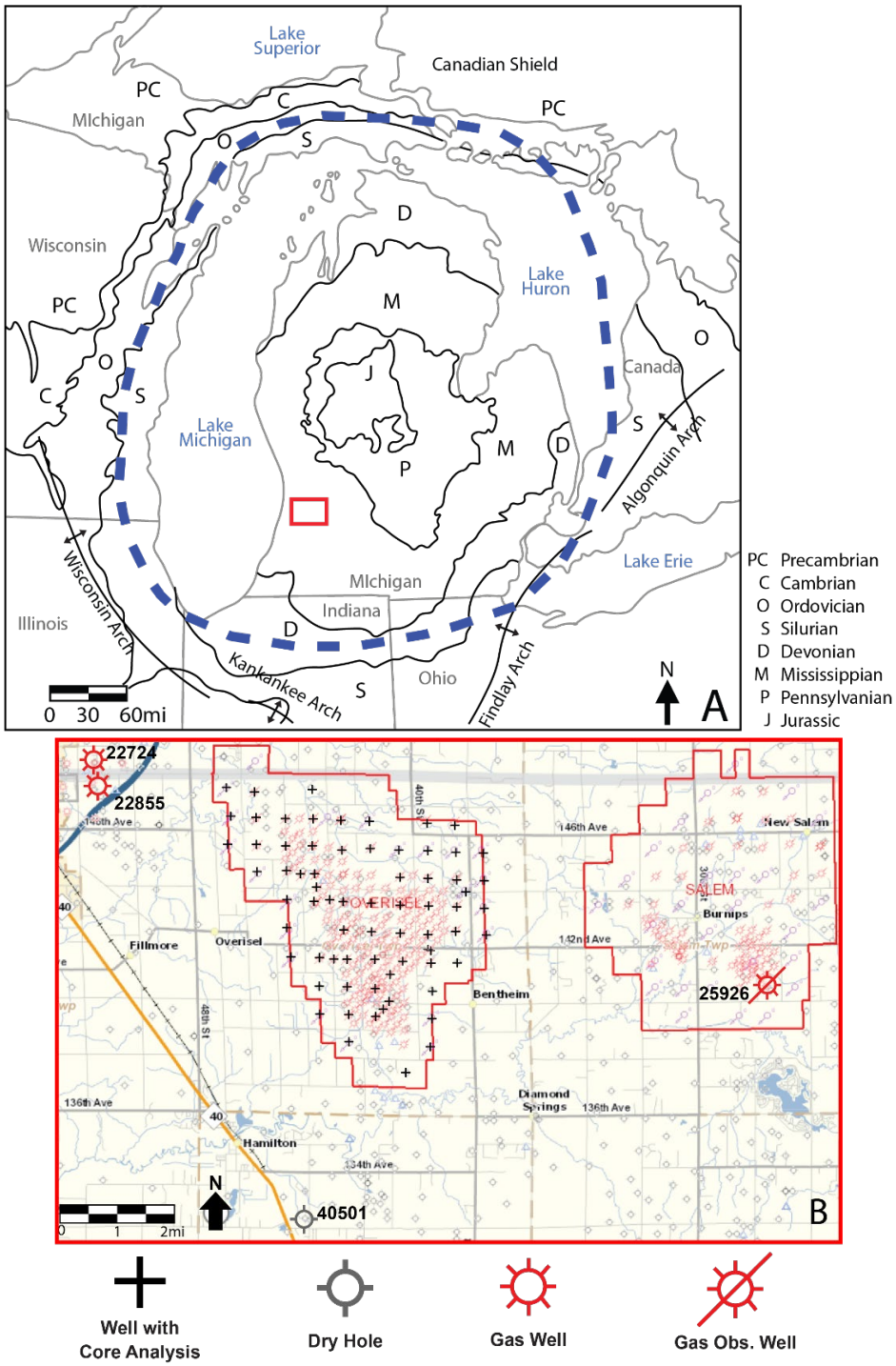

Figure 1. (A) General boundary of the Michigan Basin with location and orientation of surrounding arches. The red box highlights the gas storage fields of interest. Image modified from Catacosinos et al., 2001. (B) Outline of the Overisel and Salem natural gas storage fields with available data used in this study. Enlarged well symbols represent wells that have core available for observation. The representative permit number is present next to the wells. Black crosses represent wells with core analysis data. Image modified from the Michigan Department of Environmental Quality.

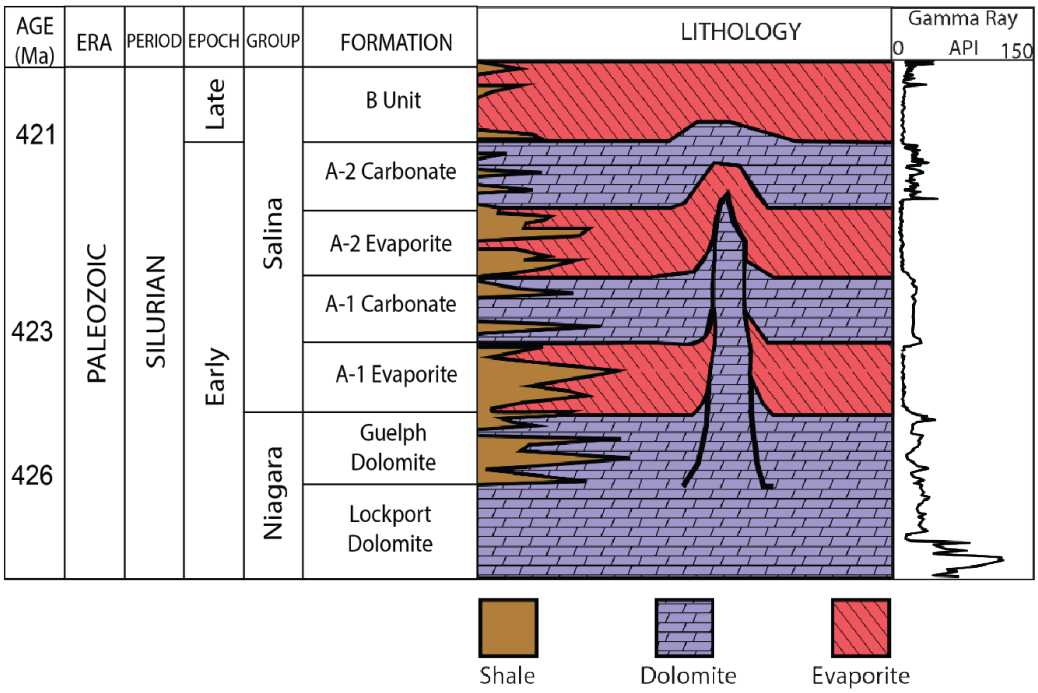

Figure 2. Stratigraphic column of the formations and groups of the upper-lower Silurian Period. Generalized lithologies, shale content, and gamma-ray signatures are provided for each of the formations. Age values are from Cramer et al., 2011. Stratigraphic terminology is from Catacosinos et al., 2001.

During late Wenlockian time, Niagaran barrier reefs rimmed the Michigan Basin to the north and south. Basin-ward, tower-like pinnacle reefs grew and formed on the shelf slope. Restriction caused from the barrier reefs in conjunction with sea-level fall during the late Silurian, generated sabkha environments in southern resulting in the deposition of the Salina A-1 Evaporite (Rine, 2015). Subsurface mapping of the Silurian formations done by Mesolella (1974) indicate that these halite salts thicken basin-ward and transition to anhydrite near reef structures and on the basin margins. A subsequent sea-level rise allowed for production of carbonate sediment on the basin margins again, leading to the deposition of the Salina A-1 Carbonate. With the basin partially restricted, the normal marine conditions of the Niagaran were not fully re-established leading to less abundant and diverse fauna within the basin interior (Mesolella,

1974). Another fall in sea-level deposited the A-2 Evaporite which eventually capped the reef structures. Like the A-1 Evaporite, the A-2 Evaporite thickens basin-ward and transitions from halite in the interior basin to anhydrite near the pinnacle reefs and basin margins (Mesolella, 1974).

Rine (2015) proposed a regressive systems tract during the A-2 Evaporite deposition that resulted in a change in sea-water chemistry in the basin that led to gypsum deposition. During early diagenesis, the gypsum was dewatered under pressure and converted to anhydrite. As the transgression continued, the dense, micritic A-2 Carbonate was deposited, filling in the antecedent topography from the earlier Niagaran Reef belt (Rine, 2015). The Salina B-Unit caps the Salina A-2 Carbonate and ranges in thickness from 50 feet around the basin margins to 475 feet in the basin center (Ells, 1967). It is a widespread unit that is composed of halite and anhydrite in the lower portions of the unit, with interbedded salt, shale, and dolomite beds in the upper portions.

The vast majority of research on the A-2 Carbonate has focused on the stratigraphic relationships with the underlying Niagaran reefs (Gill, 1973; Tremper, 1973; Budros, 1977; Lilienthal, 1974; Mesolella, 1974; Huh et al., 1977; Leibold, 1992; Rine, 2015). Ells (1967) is a report of Silurian oil and gas production from the Michigan Geological Survey that offers a general overview of the Silurian formations with structure maps, field data, production, gas analysis, and some reservoir data presented for Silurian fields throughout the Michigan Basin. Tremper (1973) is one of the few studies to describe the A-2 Carbonate using core, characterizing the formation as a non-fossiliferous, dense carbonate mud that consists of limestone in the basin center and dolomite on the basin margins. More recently, Rine (2015) used wire-line logs to distinguish the stratigraphic relationship between reef-related sediments,

including the A-2 Carbonate, to propose a sequence stratigraphic model for the southern reef trend. Stratigraphic relations suggest that the A-2 Carbonate can be correlated to the Greenfield Dolomite in Northwestern Ohio, indicating that the same carbonate sediment was deposited over the entire Michigan Basin and stretched southward over the barrier reefs that once restricted the Michigan Basin from open sea-water (Gill, 1973). In the northern part of the basin, the A-2 Carbonate thickens towards the basin interior unlike the Brown Niagaran and A-1 Carbonate. Mesolella (1974) broadly suggests that the thickening of the A-2 Carbonate in the basin interior can be attributed to physical controls, rather than biological controls, during deposition as evidenced by the lack of reef sediment.

The A-2 Carbonate generally thickens from 50 feet at the basin margins to 150 feet in the basin interior. Mesolella (1974) however acknowledges an anomalously thick northern and southern trend of the A-2 Carbonate in the Michigan Basin, where the thickness of some areas of the A-2 Carbonate is up to 200 feet thick in the absence of the underlying A-1 and A-2 Evaporites. Mesolella (1974) describes many small-scale normal displacements and structures indicative of soft-sediment deformation in the A-2 Carbonate core from a well located on the southern margin of the Michigan Basin in Eaton County. The core descriptions refer to the base of the A-2 Carbonate as consisting of carbonate rubble. Another observation was the absence of the underlying A-2 Evaporite, suggesting that dissolution of the A-2 Evaporite led to subsequent collapse of the overlying sediment during the deposition of the A-2 Carbonate. Structure maps and cross-sections of the Silurian producing fields by Ells (1967) indicate the presence of anticlinal structures in the A-2 Carbonate corresponds to regions with lenses of the A-1 Evaporite underlying the A-2 Carbonate. Subsurface mapping and brecciation features in Upper Silurian and Middle Devonian outcrops in the Northern Lower Peninsula of Michigan led to the

conclusion that "... most, if not all, salt-cored structures in Michigan are due to removal of salt by circulating ground waters" (Ells, 1967 pg.18).

Focusing on eight natural gas and oil fields in southwest Michigan, Ells (1967) suggests that the structural traps in the Silurian formations are likely due to the salt tectonics of the A-1 and A-2 Evaporite. Cores confirm that A-1 Evaporite salt is present under the Fillmore, Overisel, and Salem fields. Ells (1967) is the only study focused on the reservoir characteristics of the A-2 Carbonate, and provides some insight on porosity, permeability, and the formation, presence and configuration of structural traps. However, many of these assertions are either unsupported by data or rely on sparse and often incomplete data sets. For example, the structural maps and generalized cross sections generated for the A-2 Carbonate fields are outdated, and the lack of core analysis data and core photos presented leaves room for further study and interpretation. No study has confirmed the presence of, nor characterized the assumed fractures and fracture networks in the A-2 Carbonate. Thus, any potential role that fractures may have in enhancing natural gas storage and conveyance remains unknown. Observational data on the presence of fractures in the A-2 Carbonate is restricted to incomplete cores from outside the Overisel field, and additional methods are needed to infer the presence and influence of reservoir fractures.

Analysis of all available data for the A-2 Carbonate, along with the underlying and overlying formations is necessary to advance the current understanding of the A-2 Carbonate on both a regional and reservoir scale. The Overisel and Salem gas storage fields have extensive aerial coverage comprised of 178 wells and 102 well, respectively. The abundant well coverage allows for the generation of a high-resolution structural interpretation of both gas storage reservoirs, yet the study of geological processes that created and diagenetically altered the structure of the reservoirs is limited by well depth as all but two of the wells are restricted to the

upper 40 feet of the A-2 Carbonate. Core from locations near the Overisel field can provide insight into the depositional environment and diagenesis of the A-2 Carbonate in southwest Michigan. Petrophysical data from the Overisel field can be used to differentiate depths and well locations with more favorable primary porosity and permeability values for gas production and storage. Analysis of production and well gas flow test data can also be used to calculate formation permeability at individual well locations, and to investigate the influence of larger-scale permeability controls (such as fractures and regional lineaments) in the Overisel field.

This study maps distributions of the Silurian formations in southwest Michigan to assess the influence that each formation has on the structural and stratigraphic controls on the deposition and diagenesis of the A-2 Carbonate. A conceptual geological model for the A-2 Carbonate in southwest Michigan is then developed from a synthesis of previous studies including the A-2 Carbonate, analysis of potential analogs, subsurface mapping and stratigraphic correlations, and core observations. This model is then parameterized with high resolution core measurements of permeability and porosity from wells in the Overisel gas storage field to generate a 3D static reservoir model intended to assist in the identification and visualization of zones of higher porosity and permeability. Formation permeability estimates from isochronal single-point flow tests and production rates provide a basis for evaluating the utility of the Overisel 3D static reservoir model.

Methods

This study utilizes past literature, subsurface mapping, as well as core and thin section observations, to first develop a conceptual geologic model of the Overisel field (CGM) (Table 1). The CGM relies on the interpretation, integration, and synthesis of this data and provides a basis

for the 3D static reservoir model of the Overisel gas storage field. The static reservoir model is generated by discretizing and parameterizing the CGM with petrophysical data comprised of permeability and porosity values. The core analysis data from wells in the Salem field were not available for this study, limiting the construction of the 3D static reservoir model to the Overisel field. Methods used to generate input data to the CGM and reservoir model are further discussed in detail below. In-situ reservoir permeability at larger scales is estimated from multi-point open-flow gas tests. The potential role of fractures in enhancing permeability is inferred through comparisons of core and in-situ reservoir permeability data. Initial and post hydraulic fracturing/acidification production data and gas flow data are also used to characterize the Overisel A-2 Carbonate reservoir.

Subsurface Mapping

Archived raster wire-line logs from the Michigan Department of Environmental Quality GeoWebFace interactive website (State of Michigan, 2018a) are used to identify and correlate the stratigraphic and structural relationships of the Silurian facies. Distinct gamma-ray signatures distinguish the carbonate lithofacies from the anhydrite lithofacies (Figure 2). Tops for the carbonate formations and subsequent lithofacies are picked according to the distinct, higher gamma-ray signatures when compared to the much lower gamma-ray signatures of the evaporite formations and lithofacies. Available neutron logs are used to help distinguish the dense anhydrite lithofacies from the relatively less dense carbonate and halite lithofacies. Anhydrite lithofacies are determined by the relatively low gamma-ray signature paired with a high neutron density signature, while the halite lithofacies is determined by a low gamma-ray signature and a low neutron signature.

Table 1. Types of available data and the properties that can be used to generate both the conceptual geological model and the 3D static reservoir model.

Data Type	Properties	Model
Conceptual Geological	- Past Studies - Stratigraphic interpretations - Analog fields	Conceptional Geological
Wire-line Logs	- Stratigraphic relationships of lithofacies - Structure of lithofacies	
Core and Thin Sections	- Sedimentary structures - Diagenetic alterations - Stratigraphic relationships of lithofacies	
Core Analysis	- Porosity and Permeability - Water Saturation	3D Static Reservoir

A total of 383 gamma-ray logs and neutron logs, verified from the 4 cores, allowed for identification and delineation of the B-unit Anhydrite, A-2 Carbonate, A-2 Evaporite, A-1 Carbonate, A-1 Evaporite, and Brown Niagaran on a regional scale. A subset of 260 gamma-ray and neutron logs, along with 18 Circumferential Borehole Image Logs (CBIL), are utilized to identify the stratigraphic tops of the Silurian formations in addition to five lithofacies that comprise the A-2 Carbonate in the Overisel and Salem gas storage fields. The lithofacies are composed of the A2D1, A2D2, and A2D3 dolomite lithofacies that are separated by the A2A1 and A2A2 anhydrite lithofacies.

The identified depths of the formation and lithofacies tops are the necessary data required to generate structural maps and stratigraphic cross-sections on both a regional and reservoir scale of the formations of interest. Stratigraphic cross-sections are generated to identify the presence and lithology of the A-1 and A-2 Evaporite formations regionally in southwest Michigan, and particularly near the Overisel and Salem gas storage fields. The interpretation of the gamma-ray

and neutron logs and the resulting geological maps serve a significant role in generating structural and stratigraphic relationships that are key components in developing the CGM and ultimately the 3D static reservoir model.

Core and Thin Section Observations

No cores are available for observation from the Overisel field and only one core is available from the Salem field. Three additional cores were selected for observation given their close proximity to the Overisel gas storage field (Figure 1). Three of the cores observed in this study are incomplete with many of the lithofacies of interest absent in some cores and present in others. The Consumers Power Company S-503-E (PN: 25926) core contains only the A2D1, A2A1, and A2D2 lithofacies from a gas observation well located in the southeast part of the Salem gas storage field, just two miles from the Overisel field. The V. Rabbers Community No.1 (PN: 22855) core contains intervals of the A2D1, A2D2, A2A2, and A2D3 lithofacies. The H. Schaap Community No.1 (PN: 22474) core contains an interval of the A2D3 lithofacies. Both the V. Rabbers and H. Schaap cores were extracted from gas producing wells in the Fillmore field located approximately two miles west of the Overisel field. The PRINS 1-16 (PN: 40501) core is the only complete core that contains all the lithofacies of interest and is from a dry hole located three miles directly south of the Overisel field.

Cores are observed using hand lens to identify sedimentary structures, pore types, and diagenetic features associated with fractures, dissolution, oil staining, and salt plugging. Hydrochloric acid serves as a useful tool to identify dolomite from limestone. Rock classifications are based on the Dunham (1962) carbonate classification scheme. In addition, thin sections from different footages throughout the A-2 Carbonate are available for the PRINS well

and are observed using light microscopy. Crystal types and sizes of anhydrite and dolomite are described, along with other diagenetic features including fractures, dissolution, and salt plugging for each of the thin sections depths available. Core and thin section photos and key observations, as well as the depth at which each occurs on the corresponding gamma-ray logs for the wells used in this study are included in Appendix A.

3D Static Reservoir Modeling

Stratigraphic and structural relations of the lithofacies obtained from subsurface mapping, core and thin section observations, and past studies serve as the input data for the CGM for the Overisel gas storage field. The gamma-ray and neutron logs with the corresponding tops of the lithofacies picked were uploaded into Schlumberger's Petrel software (2015) to generate a 3D CGM that is then discretized and parameterized with porosity and permeability values from the upper 40 feet of the gas storage A-2 Carbonate reservoir facies to create the 3D static reservoir model. Model boundaries correspond to the outermost gas producing wells of the Overisel field. Two-dimensional surfaces for the B-Unit, A-2 Carbonate lithofacies: A2D1, A2A1, A2D2, A2A2, A2D3, and the base of the A-2 Carbonate are generated within the defined boundary according to the depth elevations of the lithofacies tops picked using a default convergent gridding algorithm on a 50 x 50 ft grid in Petrel (Schlumberger, 2015). Only one well penetrates the underlying A-2 Evaporite that defines the thickness of the A-2 Carbonate in the Overisel field. Thus, an average thickness of 150 feet for the A-2 Carbonate is calculated from surrounding wells that penetrate at least the A-2 Evaporite and is assigned to the model.

The generated surfaces are quality checked to remove effects of bad interpretations or noisy input data. The smoothing tool is used to remove peaks and valleys in the surfaces to

eliminate artificially intersecting surfaces and ensure that all the surfaces are geologically correct. The surfaces serve as the input data to create a 3D pillar grid that is suitable for geological modeling using the same boundary and grid size as the surfaces. The pillars are represented as vertical lines connecting the corner points of surface grids to define the 3D grid cells that ultimately determine the basic framework of the grid.

Whole core analysis data from 77 wells are used to distribute petrophysical data throughout the Overisel field (Figure 1(b)). Histograms for the porosity and permeability values for the three reservoir lithofacies are presented in Appendix B. Additionally, statistical analysis for the permeability values selected from a subset of 20 wells is performed to determine the distribution and average of the dataset and for individual lithofacies in Appendix B. An average of 10 porosity and permeability data points from core analysis were measured in the A2D1 reservoir lithofacies, 30 data points were measured for the A2D2 reservoir lithofacies, and 50 data points were measured for the A2D3 reservoir lithofacies for each of the 77 wells that has core analysis data. Thus, the same number of proportional layers for each of the reservoir lithofacies between the surfaces in the static reservoir model are created so that the distribution of core analysis data is representable. No porosity or permeability measurements have been recorded for the B-Unit, A2A1, and A2A2 lithofacies, and thus one layer is made for each of the anhydrite lithofacies with assigned 0% porosity and 0.0 mD permeability values to reflect this lack of data.

The porosity and permeability values are then upscaled so that a there is a single value for a given cell using a arithmetic and geometric average, respectively. Once the wells are upscaled, porosity and permeability values are distributed throughout the reservoir lithofacies zones by kriging. A spherical variogram with a total sill of 1.0 and 0.0001 nugget is used with the

recommended maximum and minor horizontal ranges (x_{min}, x_{max}, y_{min}, y_{max}) set to half the smallest dimension of the model boundary using the equation: $\frac{Min\left((Xmax-Xmin),(Ymax-Ymin)\right)}{2}$ The vertical kriging range is set to 2 times the average cell height for each of the corresponding zones.

Open-Flow Potential Test Permeability

Formation permeability is calculated using the multi-point open-flow potential test (OFPT) methods described in Matthews and Russell (1967). The OFPT provides estimates of permeability for tight gas reservoirs for a series of transient measurements of flowing bottom-hole pressures made at various flow rates. The method consists of first plotting:

$$\frac{p_i - p_{wfn}}{q_n}$$

versus

$$\sum_{j=1}^{n} \left(\frac{q_j - q_{j-1}}{q_n}\right) log(t_n - t_{j-1})$$

to yield a linear relationship with a slope:

$$m' = \frac{28{,}958\ \mu_g B_g}{k_g h}$$

where,
p_i = Initial pressure (psia),
p_{wfn} = Bottom-hole flowing pressure (psia),
q_n = flow rate (MCF/day),
t_n = time of test (hr),
t_j = time elapsed (hr),
μ_g = viscosity (cp),
Bg = formation volume factor of gas,

k_g = permeability,
and h = pay zone thickness (ft).

The permeability thickness, $k_g h$, product can be determined from the slope, m'. Permeability, k_g, can then be solved from dividing the known pay thickness of the well. The formation volume factor describes the gas volume change from reservoir to surface conditions and is computed from the relationship (SPE, 2015): $Bg = \frac{14.65\ Tz}{519.67\ p}$. Both reservoir temperature, T, and absolute pressure, p, are recorded during the well test. The gas compressibility factor, z, specific to the Overisel reservoir was provided by Consumers Energy. Viscosity, μ_g, is the only variable estimated from literature values, with most natural gas viscosities ranging from 0.01 to 0.03 cp (SPE, 2015) thus an average value of 0.02 cp is used in this study.

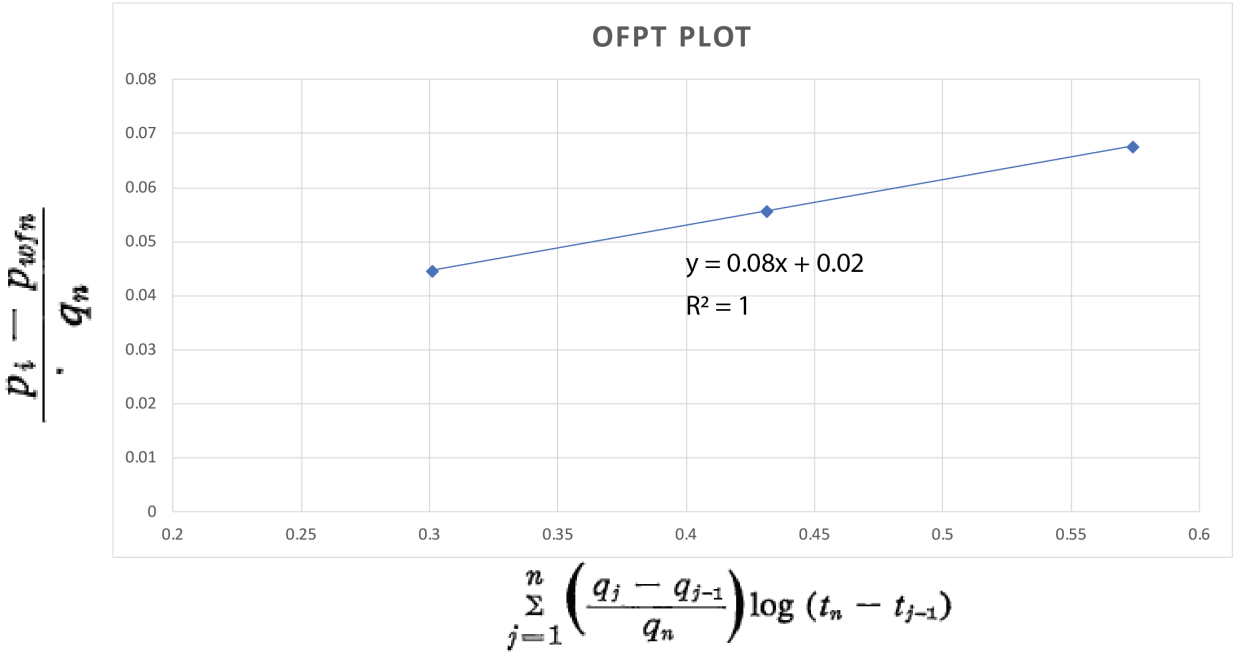

Figure 3. Example OFPT plot from the Consumers Power Company 48 (PN: 21435) well with a slope of 0.084 and an R^2 value of 1.00.

The OFPT method is used to estimate formation permeability for all available wells in the Overisel gas storage field. This is comprised of 30 wells that contain core analysis data and 12 additional wells that lack core analysis data. It is assumed that the A2A1 and A2A2 anhydrite lithofacies do not contribute to fluid flow in the reservoir, so the thickness of those intervals is subtracted in the computation of pay zone thickness, *h*. Intervals that have core analysis permeability values of 0.0 mD are also subtracted from the pay zone thickness because it is assumed those intervals do not contribute to flow. The OFPT method serves as a valuable method to calculate formation permeability on a borehole scale relative to permeability calculated on individual core samples, possibly identifying larger fractures that contribute to flow.

Production and Flow History Data

Initial and post acidification/hydraulic fracturing production data for the Overisel field is available from numerous scanned drillers logs from the Michigan Department of Environmental Quality GeoWebFace (State of Michigan, 2018a). A total of 96 wells have initial production data available in the database, while 44 wells had post acidification/hydraulic fracturing production data. Both forms of production data can be used to interpolate and contour the volumes of gas produced per day at each well to generate production maps of the Overisel field. Initial production wells with only a recorded show of gas are assigned values of 100 Mcf. The amount of acid and hydraulic fracturing sand used on each well is also compiled. Almost all acidized-only wells were treated with 2000 gal of hydrochloric acid, with a small subset of wells treated with up to 10,000 gal of HCl. All hydraulically fractured wells were treated with 3,600 lbs. to 4,200 lbs. of sand proppant along with 2,000 gal of HCl.

Absolute open-hole flow and test flow rates from the Overisel field were compiled from 124 Consumers Energy gas observation wells to identify wells with higher flow rates. Absolute open-hole flow measures the flow of natural gas against atmospheric pressure, whereas the test flow rate measures the flow of natural gas against a controlled bottom-hole pressure. Both measurements have units of million cubic feet of gas per day (MMCF/day). These measurements have been recorded annually from 1961 to present day. Averages of the annual measurements for absolute open-hole flow and test flow rates are computed for each well. These absolute open flow and test flow averages are contoured to create flow rate maps for the Overisel field.

Results

Subsurface Mapping

The upper surface of the A-2 Carbonate delineated from tops picked from all available wire-line logs is illustrated in Figure 4 for the Overisel and Salem gas storage fields. The Overisel field has an average subsea true vertical depth (SSTVD) of approximately -1990 feet. The southern part of the field is structurally highest with a high of -1915 feet. A local high of -1709 SSTVD exists in the northeast and is likely caused by the presence of a Brown Niagaran reef beneath the Salina Group units according to the drillers report from the well that discovered this structure. The Salem field is structurally lower with an average SSTVD of -2095 feet. Structural elevations for the Salem field are more heterogeneous with two depressions on the western edge of the field and a large circular depression in the center of the field.

A regional structure map of the A-2 Carbonate in southwest Michigan is generated from wells that penetrate at least the top of the A-2 Carbonate (Figure 5). Wells that penetrate the A-1 Evaporite are shown with the corresponding salt or anhydrite lithology present at that location.

The A-2 Carbonate has a generally constant change in elevation from -900 feet SSTVD at the basin margin in the southwest to -3800 feet SSTVD towards the basin center in the northeast. Local structural highs anomalous to the general dip in the A-2 Carbonate occur where the producing Overisel, Salem, and Fillmore fields are located. The local highs are consistent with the presence of A-1 Evaporite Salt underlying the A-2 Carbonate. The A-1 Evaporite Salt and Anhydrite boundary indicated by the blue line, marks an abrupt transition from an average of 140 feet of salt to an average of 15 feet of anhydrite. Generally, the boundary occurs on a linear trend striking from northwest to southeast, although the strike of the boundary follows the A-1 Anhydrite where the reported structural lineaments occur (State of Michigan, 2018a).

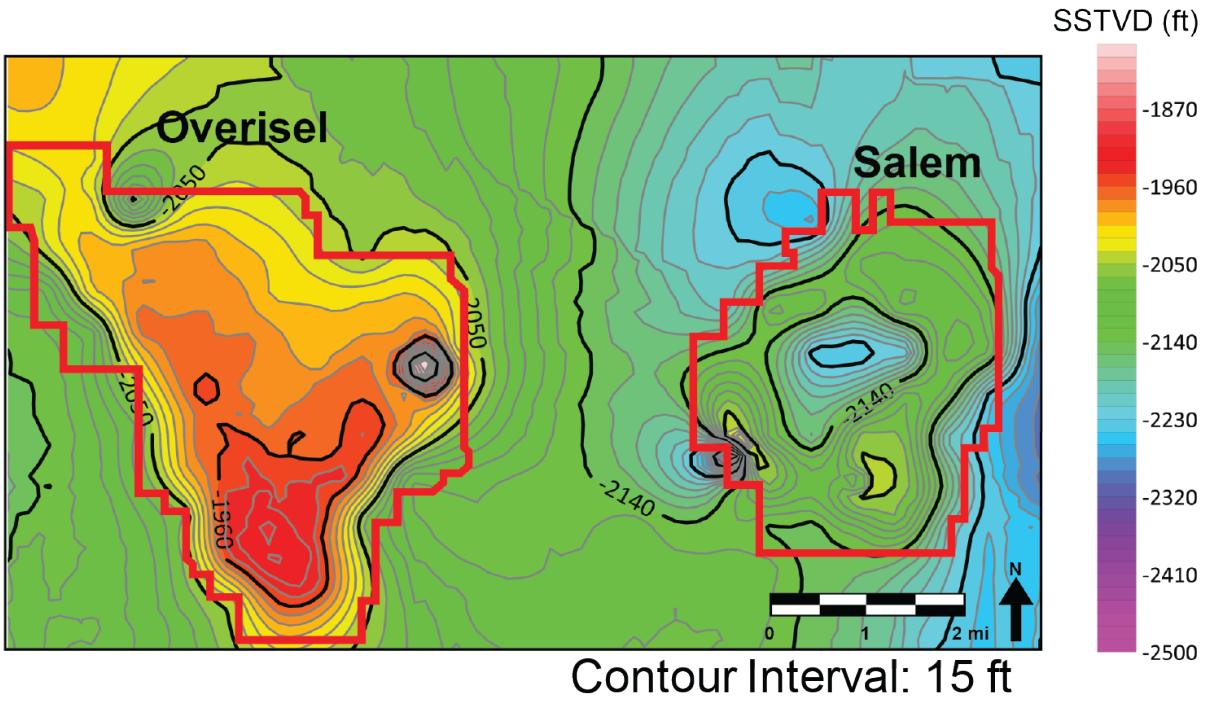

Figure 4. A-2 Carbonate structural map for the Overisel and Salem fields generated from tops picked using gamma-ray and neutron wire-line logs. The map illustrates the complex structure of the A-2 Carbonate within the gas storage fields.

Figure 6 displays the cross-section for the A to A' transect in Figure 5. The west-east oriented cross-section shows the relationship between the A-1 Evaporite salt and anhydrite presence according to gamma-ray signatures. The A-1 Evaporite salt occurs along the transect in pillows that abruptly transition into thin anhydrite beds rather abruptly. Thicknesses of the overlying sediments remain constant throughout the transect, while the underlying Brown Niagaran exhibits more complex structure with varying relief. The thinner A-1 Evaporite Anhydrite facies is present on top of the relatively higher structures of the Brown Niagaran.

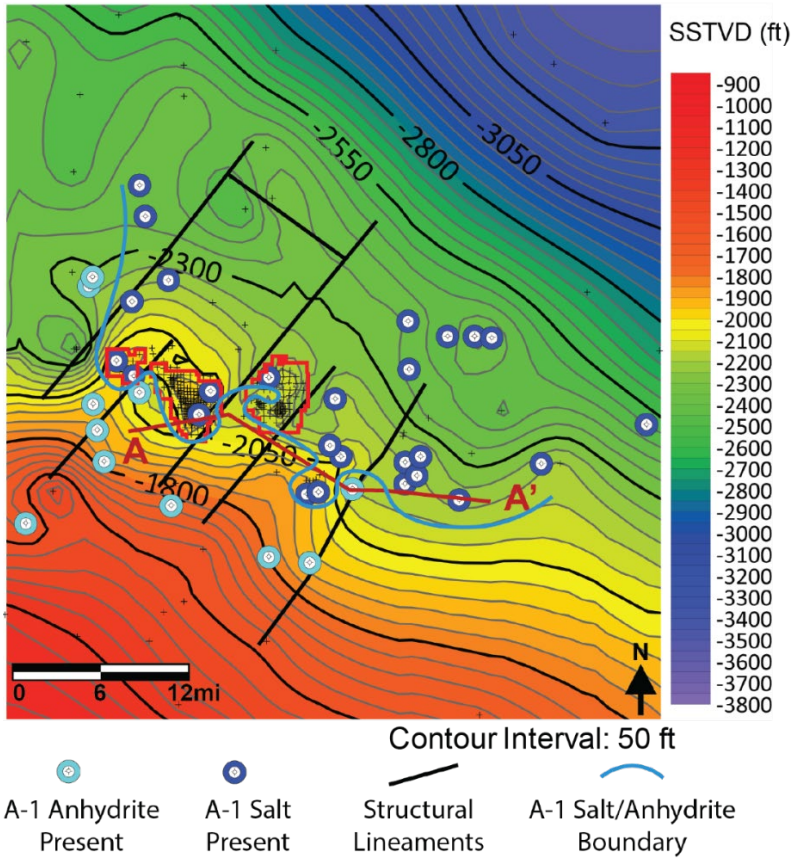

Figure 5. Regional A-2 Carbonate structure map generated by interpolating top surface elevations (black crosses) marked from gamma-ray and neutron logs. The blue line denotes the A-1 Salt/Anhydrite boundary based on the presence of salt (dark blue) or anhydrite (light blue) in boreholes. Red boundaries represent natural gas producing A-2 Carbonate fields. Mapped structural lineaments are from the Michigan Department of Environmental Quality GeoWebFace (State of Michigan, 2018a).

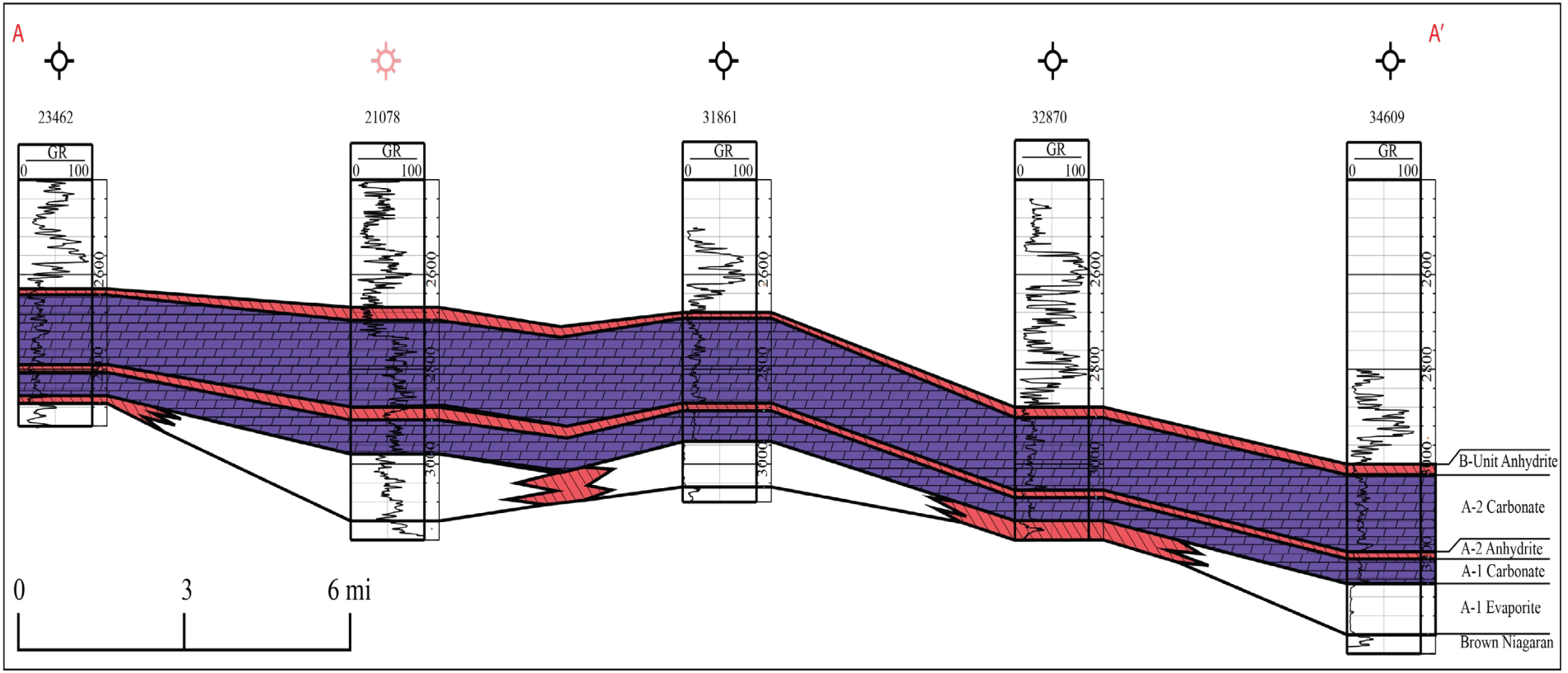

Figure 6. Cross-section A-A' from Figure 5 showing the distributions of the Silurian formations in southwest Michigan. The A-1 Evaporite Salt occurs in pockets that abruptly transition to A-1 Anhydrite. Relief of the Brown Niagaran varies considerably.

Core and Thin Section Observations

The A2D1 and A2D2 lithofacies observed from the Consumers Power Company S-503 (PN: 25926) gas observation well is mostly composed of dolomudstone interbedded with thinner intervals of dolowackestone. The mudstone intervals contain dense homogenous dolomitic mud with compacted nodular anhydrite and dark anhydrite laths present. The dolowackestone intervals vary in grain size and composition. Multiple intervals of the A2D2 lithofacies have wackestone that has sub-rounded imbricated dolomite clasts with compacted, nodular anhydrite and muddy dolomite stringers present. Other intervals of the dolowackestone have much more angular grains, separated by fractures filled with anhydrite laths. Nodules of anhydrite vary in size from small nodules of 1 cm to massive anhydrite beds up to 1 ft thick that appear to displace the carbonate mud. Vertical and horizontal, wavy stylolites are present throughout the core. The stylolites commonly wrap around dolomite clasts in the wackestone intervals.

The A2D1 lithofacies observed from the V. Rabbers Community No.1 (PN: 22855) well is largely composed of light grey, dolomudstone and dolowackestone with small intervals of dolopackstone. Intervals with abundant vuggy porosity and oil staining occur in the dolowackestone intervals of the A2D2 lithofacies. Vuggy porosity also exists in the micritic intervals but is not nearly as abundant as the brecciated and wackestone intervals. The dolomite intervals vary in size and composition with angular clasts as large as 2.0 inches in diameter that are a grain supported dolopackstone, to rounded clasts as small as 1 cm in diameter that are supported in an anhydrite matrix. Stylolites are abundant in both the micrite and wackestone intervals. The stylolites occur at vertical, horizontal, and inclined orientations and are mostly wispy and wavy. Other horizontally oriented and sutured, sharp peak stylolites exist but are less common than the wavy stylolites. Open, vertical fractures that vary in length and aperture are

common throughout the core and cut across and displace bedding planes and stylolites. Other smaller fractures are observed to be concentrated around stylolites. Anhydrite nodules that are up to 3 inches wide occur at the top of the A2D1 lithofacies, with intervals containing very thin anhydrite laths occurring deeper in the A2D2 lithofacies. The A2D3 lithofacies is mostly a dense dolomicrite with abundant horizontal and inclined stylolites. Vertical fractures cut through what appears to be a stromatoporoid at the top of the A2D3 lithofacies.

The H. Schaap Community No.1 (PN: 22474) well core is composed of interbedded dolomicrite, dolopackstone, and dolorudstone throughout the A2D3 lithofacies that is available for observation. Intervals of dolomicrite have large vugs that are partially filled with sucrosic dolomite. Other areas of vuggy porosity exist throughout the A2D3 lithofacies in the dolorudstone intervals that have abundant stylolites and brecciation. The clasts in the packstone and rudstone range from angular to sub-angular and vary from 1 cm wide to 2 inches wide. Some clasts appear to be imbricated with others having sutured contacts. A thin brecciated zone with imbricated clasts has anhydrite laths spread between the clasts. Abundant stylolites occur throughout the core. Horizontal stylolites are most common, with fewer interconnected vertical stylolites. Most stylolites are wavy in form with fewer stylolites having sharper sutured peaks. Vertical fractures cut across and displace the stylolites and different beds of the carbonate rock. Some of the fractures are partially filled with anhydrite laths, while others are completely open. The fractures vary in length from 1 inch up to 6 inches.

The A2D1 lithofacies in the PRINS 1-16 (PN: 40501) well core is composed of dolomicrite with abundant horizontal and slightly inclined oriented stylolites. There is a large vertical fracture that is filled with anhydrite laths that cuts through the stylolites. Anhydrite cement is also present in fractures that are connected to the stylolites. The anhydrite laths are

disseminated throughout the core and also occur preferentially associated with stylolites. The A2D2 and A2D3 lithofacies are composed of dolomicrite interbedded with thinner beds of dolowackestone, dolopackstone, and dolograinstone. Decussate dolomite textures (Gardner, 1974) are present in what could be remnant algal mats at the top of the A2D2 lithofacies. Anhydrite laths are spread throughout the decussate dolomite and form a network of laths that cut across the horizontal stylolites. Stylolites are common in the dolomicrite intervals. The dolograinstone bed has sub-angular, imbricated clasts with anhydrite laths filling the matrix around the clasts. The wackestone and packstone beds have compacted, sub-angular clasts that are supported in a muddy matrix. Zones with large vertical fractures that are filled with anhydrite laths are spread throughout the A2D2 and A2D3 lithofacies.

The thin sections of the A2D1 lithofacies from the PRINS core show that the A2D1 lithofacies is composed of finely crystalline, micritic dolomite with nodular anhydrite spread throughout the muddy dolomite matrix. There are some larger, subhedral dolomite rhombs spread throughout the muddy matrix but are very scarce. More finely crystalline, micritic dolomite is present at the top of the A2D2 lithofacies but the larger, subhedral dolomite rhombs are much more common with abundant porosity around the rhombs. Anhydrite cement fills some of the porosity around the dolomite rhombs. There are open, vertical microfractures that cut through the dolomite matrix with some anhydrite cement partially filling the void space. The thin section samples of the A2D3 lithofacies deeper in section are composed of more finely crystalline, micritic dolomite with fewer subhedral dolomite rhombs present in the muddy matrix. Horizontal stylolites contain small anhydrite nodules. Much larger anhydrite nodules are present throughout the lower A2D3 lithofacies. One horizontally oriented and partially open

fracture is present and cuts across the dolomite matrix, terminating into a large anhydrite nodule. The larger anhydrite nodules contain larger dolomite rhomb inclusions.

Core Analysis

Figure 7 displays permeability values for each of the reservoir lithofacies versus depth from the top of the A-2 Carbonate for 20 wells in the Overisel field. The permeability measurements are rarely above 10.0 millidarcy (mD) with 96% of the measurements below 5.0 mD and a geometric average of 1.2 mD. The statistical analysis in Appendix B indicates that permeability values for each reservoir lithofacies and combined dataset (n=565) fit a lognormal distribution with a mean of 1.1 mD. Porosity values for each of the reservoir lithofacies versus depth for the same 20 wells in the Overisel field are shown in Figure 7. These values are normally distributed within a range from 1 to 20% with an average of 9.9% (Appendix B).

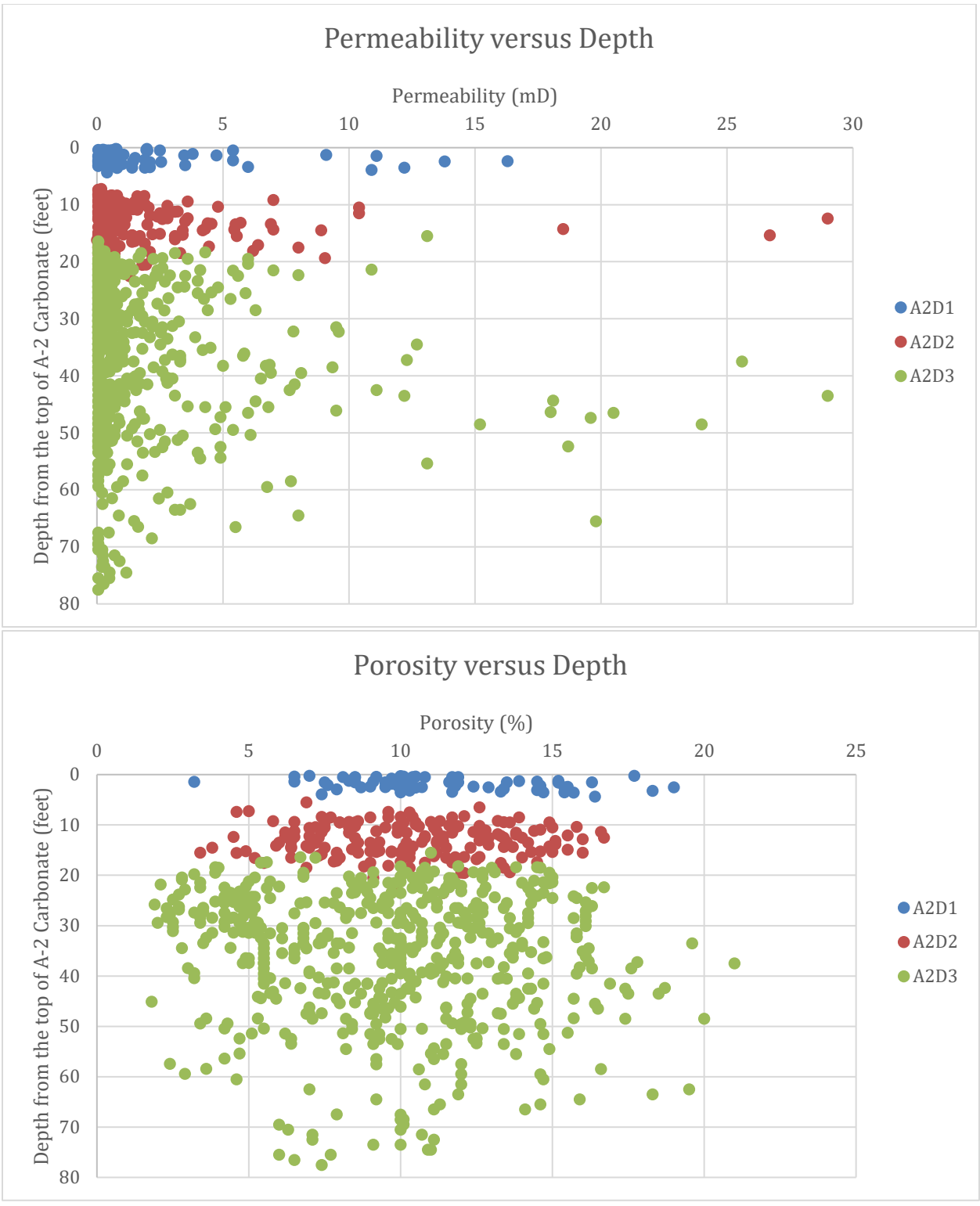

Figure 7. Overisel reservoir lithofacies permeability (top) and porosity (bottom) as a function of distance from the top of the A-2 Carbonate.

3D Static Reservoir Modeling

Map views of the average permeability for the A2D1, A2D2, and A2D3 reservoir lithofacies of the A-2 Carbonate are displayed in Figure 8, along with north-south and east-west trending cross-sections of the distributed permeability values. The map view of the A2D1 lithofacies shows a zone of higher permeability located on the western half of the Overisel field. Zones of nearly 0.0 mD (note that the permeameter testing method cannot distinguish permeability values lower than 0.001 mD) are located on the northern and southern margins of the field. The map view of the A2D2 reservoir lithofacies shows a zone of higher permeability in the northwest of the Overisel field and another near the middle of the field. These two zones are surrounded by permeability values lower than 0.1 mD. The map view for the A2D3 permeability shows higher values compared to the other two reservoir lithofacies. Values of 4.0 to 8.0 mD occur on the southern and western portions of the field and exhibit a northwest striking trend across the Overisel field.

Cross-sections in Figure 8 show that the permeability values are greater in the structurally higher parts of the reservoir. Three high permeability zones are apparent from the 3D static reservoir model. One zone is present just above and below the A2A2 lithofacies in both the north-south and east-west cross-sections. Another zone of high permeability exists approximately 35 feet from the top of the A-2 Carbonate in the A2D3 lithofacies in the southern part of the Overisel field.

Figure 9 displays the same map views of the average porosity values for the three reservoir lithofacies distributed along north-south and east-west cross-sections. The map view of the A2D1 lithofacies shows consistent porosity values around 8.0% throughout the Overisel field. Higher values around 12% porosity are present near the known pinnacle reef in the

northeast. The A2D2 lithofacies has a similar average porosity around 8.0% and has two zones of porosity up to 20% in the southeastern and northwestern parts of the Overisel field. Higher average porosity values around 16% occur in the A2D3 reservoir lithofacies in the southern and western parts of the field and continue to trend to the northwest.

Both cross-sections indicate that porosity is fairly uniform throughout the Overisel gas storage reservoir. However, higher porosity values occur near the structurally higher southern part of the field in all three reservoir lithofacies. Similar to permeability, one zone of high porosity is present just above and below the A2A2 lithofacies in both the north-south and east-west cross-sections. Another zone of high porosity exists approximately 35 feet from the top of the A-2 Carbonate in the A2D3 lithofacies in the southern part of the Overisel field.

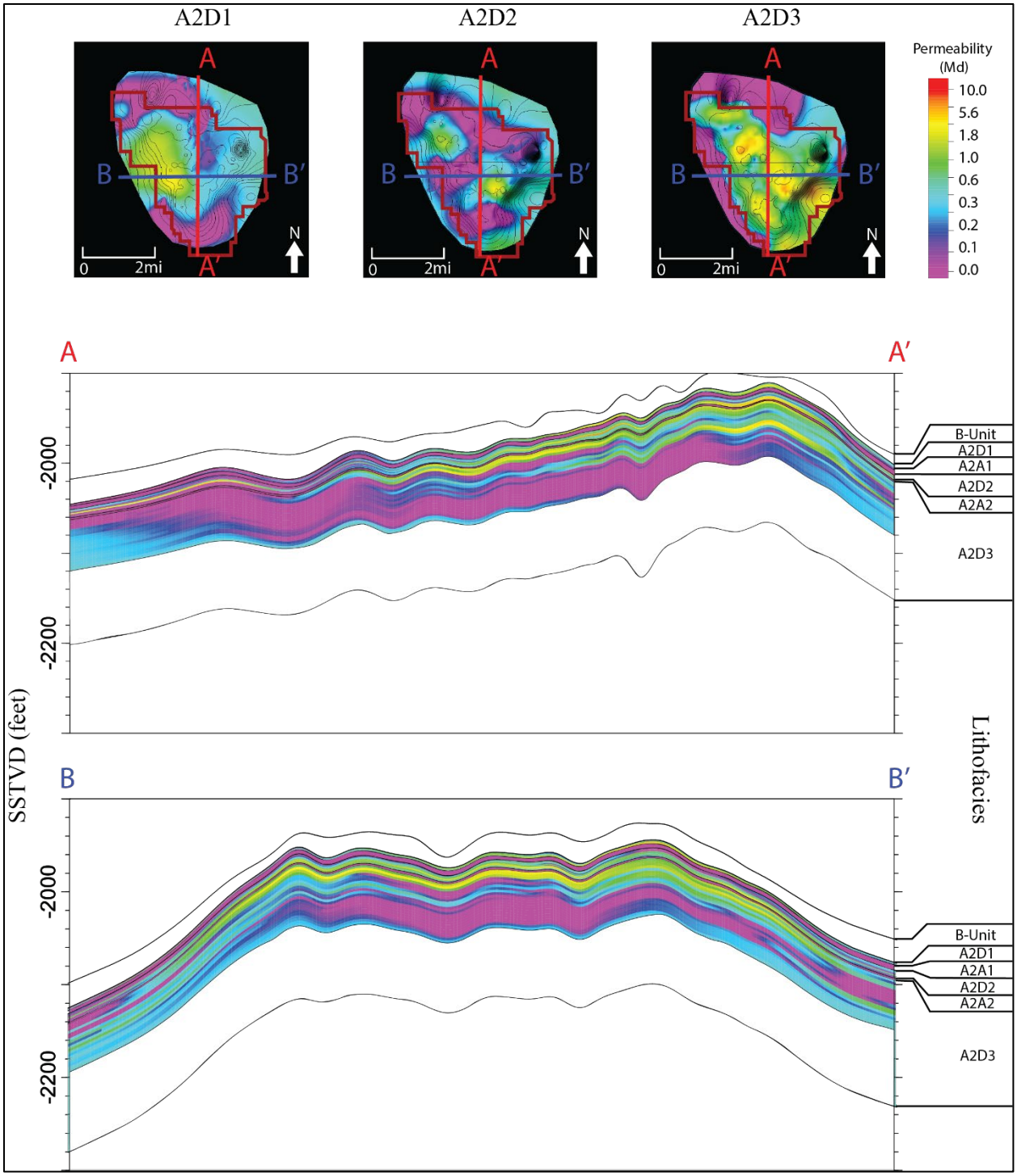

Figure 8. Permeability results from 3D static reservoir modeling. Map view (top) of the Overisel field with the average permeability of the three dolomite reservoir lithofacies. North-South (A to A') and East-West (B to B') cross sections of the Overisel field illustrate the permeability variability within the five A-2 Carbonate lithofacies.

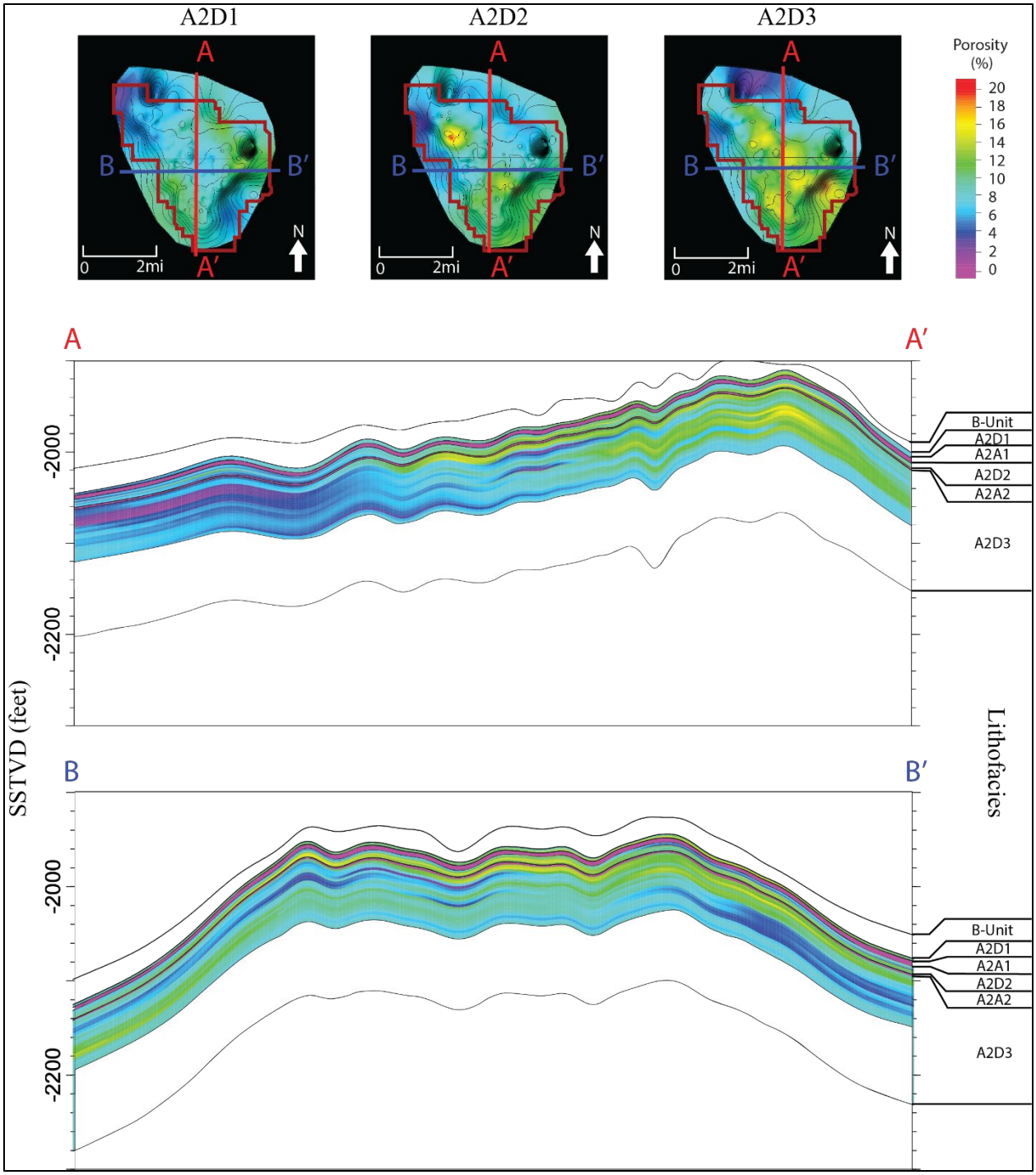

Figure 9. Porosity results from the 3D static reservoir modeling. Map view (top) of the Overisel field with the average porosity of the three dolomite reservoir lithofacies. North-South (A to A') and East-West (B to B') cross sections of the Overisel field illustrate the porosity variability within the five A-2 Carbonate lithofacies.

Open-Flow Potential Test Permeability

The OFPT permeability estimates with the corresponding geometric mean of the core permeability values are shown in Table 2. OFPT permeability estimates for additional wells lacking core permeability are shown in Table 3. The R^2 values indicate the strength of the correlation in the linear regression used to compute the slope *m'* (Figure 3) and provide a measure of the reliability of the OFPT estimates. On average, the OFPT permeability values are 500% or one half-order of magnitude greater than core permeability values for all wells. Potential correlation between OFPT and core permeability was explored using the 18 wells with a calculated R^2 value above 0.75 for the OFPT permeability analysis. To ensure a proper comparison, the geometric mean of core values was computed for the open interval (or pay zone) of each well. The analysis showed no correlation ($R^2 = 0.08$) or discernible relationship between the core and formation permeability.

Production and Flow History

Figure 11 shows contoured initial and post hydraulic fracturing/acidizing production data and contoured flow rate test average and absolute open hole flow measurements. The initial production map indicates that the most productive gas wells are in the southern part of the Overisel field and initially produced as much as 1,600 Mcf individually. Six productive wells in the northwest part of the field initially produced as much as 1,300 Mcf individually. Other wells that initially produced lower amounts of natural gas are distributed throughout the Overisel field, and wells with only a show of natural gas outline the field boundary. Post hydraulic fracturing/acidizing production data is more limited but show a significant increase in natural gas as expected.

Table 2. Results of the OFPT permeability calculations in comparison to core analysis permeability.

Well	*Bg*	*h* (feet)	*m'*	R^2	$k_g h$	k_g (mD)	*Core k (mD)*	*% Difference*
153	1.2E-02	38	2.0E-01	0.20	35	0.9	0.5	129
156	1.1E-02	44	5.0E-02	0.36	122	2.8	0.6	472
136	1.1E-02	70	7.3E-03	0.98	839	12.0	1.2	24
161	1.2E-02	20	1.5E-01	0.54	45	2.2	2.9	109
110	9.7E-03	23	2.4E-01	0.90	23	1.0	0.9	2140
113	1.0E-02	32	2.3E-02	0.73	257	8.0	0.6	2608
131	1.1E-02	40	3.7E-02	0.87	170	4.3	0.7	6156
127	1.0E-02	37	5.8E-02	0.75	100	2.7	2.0	174
111	1.0E-02	29	7.1E-02	0.87	82	2.8	1.6	153
119	1.1E-02	30	1.8E-01	0.46	34	1.1	0.7	91
211	1.3E-02	32	6.5E-02	0.98	117	3.7	2.0	20
188	1.3E-02	25	2.0E-01	0.94	38	1.5	1.2	24
179	1.4E-02	22	6.1E-02	0.64	133	6.0	2.9	109
177	1.4E-02	30	1.4E-02	0.43	595	19.8	0.9	2140
154	1.4E-02	30	1.8E-02	0.00	461	15.4	0.6	2608
135	1.0E-02	35	3.6E-03	0.66	1612	46.1	0.7	6156
140	1.0E-02	39	2.8E-02	0.94	210	5.4	2.0	174
139	1.0E-02	39	3.6E-02	0.97	159	4.1	1.6	153
120	1.0E-02	41	1.0E-01	0.20	57	1.4	0.7	91
130	1.0E-02	28	8.9E-02	1.00	68	2.4	2.0	20
105	1.0E-02	31	3.2E-01	0.75	18	0.6	0.7	-16
106	1.0E-02	33	1.8E-01	0.79	32	1.0	0.9	6
114	1.2E-02	32	8.7E-01	0.96	8	0.2	0.4	-34
118	1.0E-02	20	1.6E-01	0.60	37	1.9	0.3	524
122	1.0E-02	36	2.9E-02	0.87	203	5.6	0.9	508
124	1.1E-02	37	3.3E-01	0.91	19	0.5	0.3	81
125	1.0E-02	54	3.8E-01	0.53	16	0.3	2.1	-86
128	9.9E-03	45	9.2E-02	0.78	62	1.4	1.3	11
129	1.0E-02	57	5.6E-02	0.38	105	1.8	0.9	106
132	1.0E-02	24	8.8E-03	0.99	687	28.6	1.4	1897
					Average	**6.9**	**1.1**	**507**

Wells that have been hydraulically fractured with sand and acidized in the southwest and the middle parts of the Overisel field have produced as much as 24,000 Mcf. Acidized wells have produced on average around 3,000 Mcf. Both the initial and post hydraulic fracturing/acidizing production plots indicate the southern portion of the Overisel field is the most productive.

Table 3. Results of the OFPT permeability calculations for additional wells lacking core analysis permeability.

Well	Bg	h (feet)	m'	R^2	$k_g h$	k_g (mD)
221	1.2E-02	49	3.0E-02	0.03	230	4.7
219	1.2E-02	50	8.4E-02	1.00	85	1.7
218	1.5E-02	98	5.8E-03	0.49	1504	15.3
216	1.4E-02	40	2.1E-02	0.75	376	9.4
210	1.7E-02	35	3.8E-02	0.95	257	7.3
203	1.7E-02	36	1.1E-02	0.90	871	24.2
195	1.3E-02	29	7.1E-02	0.90	109	3.8
190	1.5E-02	39	2.2E-01	0.80	40	1.0
229	1.4E-02	30	2.6E-02	0.98	322	10.7
233	1.5E-02	43	1.9E-02	0.47	463	10.8
235	1.4E-02	31	1.4E-01	0.78	62	2.0
239	1.7E-02	35	9.5E-02	0.97	103	2.9
					Average	**5.3**

Flow rate test measurements are highest in the southern and the middle northwest parts of the Overisel field. Wells located in the southern part of the field have rates exceeding 1,800 Mcf per day, whereas wells located in the middle northwest reach upwards of 1,200 Mcf per day. The wells with the highest flow rates appear to trend towards the northeast and to the northwest. The absolute open hole flow shows similar trends with the highest natural gas amounts measured at nearly 40,000 Mcf per day in the southern and middle northwest parts of the Overisel field. The same northeast and northwest trends that appear in the flow rate test measurements are present in the contoured absolute open flow rates.

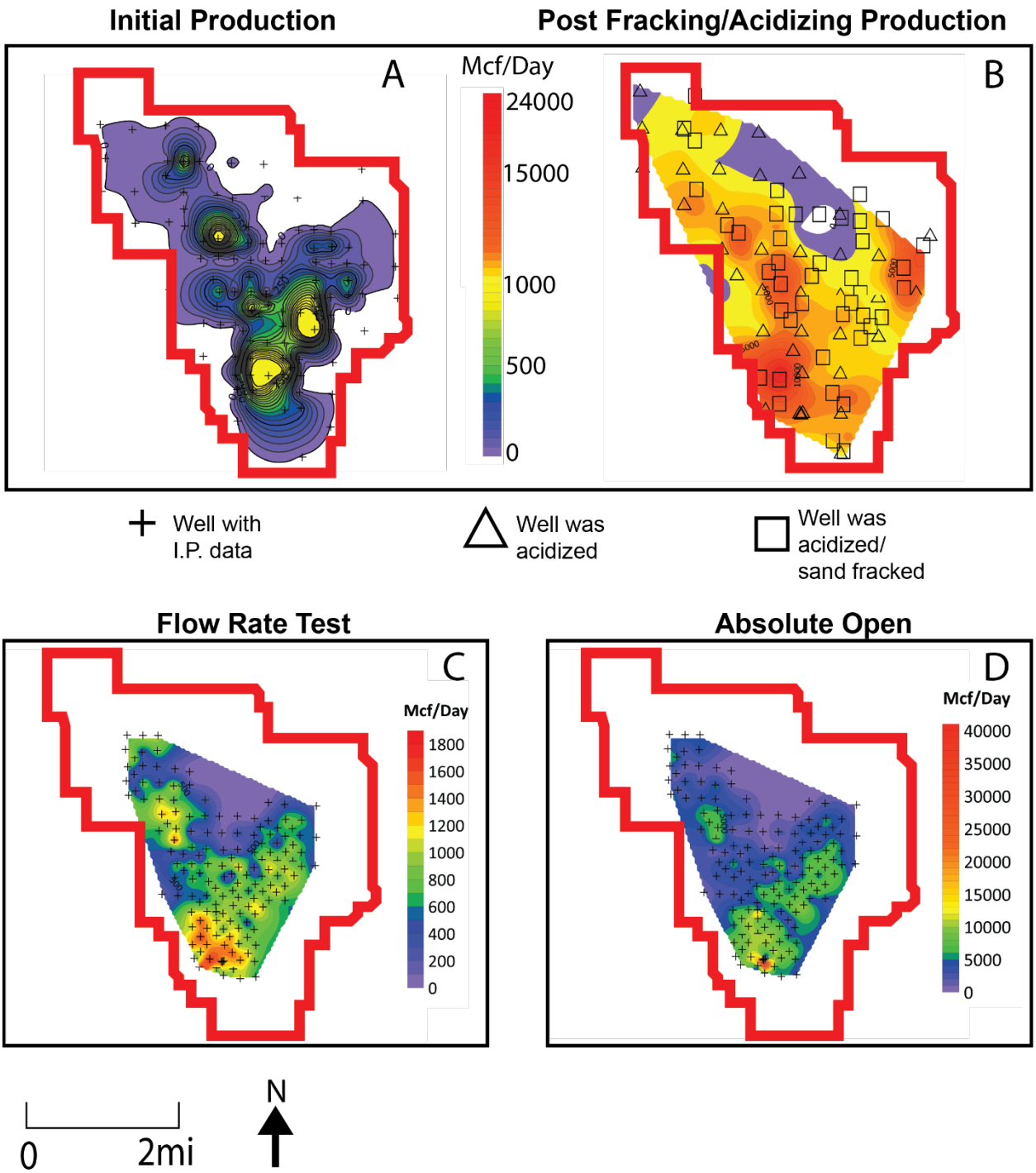

Figure 10. Initial (A) and post acidizing/hydraulic fracturing (B) production contoured maps from production data. Average flow rate test (C) and absolute open hole flow rate (D) contoured maps from single day measurements recorded annually for the Overisel field. The production maps are measured in Mcf of gas and the flow rate maps are measured in Mcf per day.

Discussion

Structural and Stratigraphic Controls

The natural gas producing A-2 Carbonate fields are associated with higher structures that have underlying A-1 Salt present as indicated by Figure 4 and 5. The A-1 Salt abruptly thins into A-1 Anhydrite on the basin margin running along the southern border of the producing A-2 Carbonate fields. The abrupt transition from salt to anhydrite is referred to as the "leach-back" edge caused by the dissolution of salt presence (Harrison and Voice, 2017). The boundary of the A-1 Salt appears to be linked to the location of known structural lineaments in southwest Michigan (Figure 4). Dominant orientation of the structural lineaments is perpendicular to the northwest trending, failed Fort Wayne Rift system that has a parallel strike to the Overisel, Salem, and Filmore A-2 Carbonate field locations (Stein et al., 2018). The underlying Brown Niagaran has varying relief (Figure 6), suggesting that underlying features contribute to the structure of the A-2 Carbonate natural gas producing fields, in addition to the presence of A-1 Evaporite salt. However, it is impossible to know if varying sedimentation rates of the Brown Niagaran or further structure from underlying Ordovician, Cambrian, or Precambrian rock created the structure of the Brown Niagaran without any knowledge of the formation thickness. It is possible that structure from the failed Fort Wayne Rift played a vital role in the structure of the A-2 Carbonate in southwest Michigan. Reactivated basement faults and fractures along the reported structural lineaments could act as fluid conduits that convey meteoric water downward to the A-1 Salt or deeper fluids from below, enhancing rates of salt dissolution of the A-1 Salt and leading to increased structural relief of the A-2 Carbonate at the adjacent Overisel, Salem, and Fillmore field locations.

Depositional and Diagenetic History

The depositional environment and diagenetic events, and the relative timing of events are inferred from sedimentary and diagenetic textures and features in core and thin sections. The A2D1, A2D2, and A2D3 lithofacies observed in the cores and thin sections used in this study are predominantly composed of dolomudstone sediment that are non-facies selective, exhibit intervals with fractures, and are interbedded with dolowackestone, dolopackstone, dolograinstone, and dolorudstone intervals that are chaotically brecciated. Laths of anhydrite are commonly spread throughout the cores with intervals of nodular anhydrite present as well. The textures and lithofacies observed in the cores resemble the Middle Devonian Richfield Member of the Lucas Formation that was described by Gardner (1974).

The massive dolomicrite intervals are interbedded with the relatively thick anhydrite beds that make up the B-unit, A2A1, A2A2, and A-2 Evaporite lithofacies suggesting that the A-2 Carbonate was deposited in a restricted, arid tidal flat environment dominated by lagoonal and sabkha sedimentation. A quasi-contemporaneous model proposed by Mesolella (1974), in which the carbonate and evaporite depositional settings are very close in time but not synchronous for the Silurian formations, agrees with the A-2 Carbonate and subsequent lithofacies observed in core and thin sections. Gardner (1974) describes a typical cycle for the Richfield dolomite, a possible analog to the A-2 Carbonate, that is observed in numerous cores throughout Michigan. The cycle suggests a penecontemporaneous relationship between the carbonate mud intervals and evaporite intervals in vertical succession. Subtle changes in sea-level in conjunction with the restriction from the topography left by surrounding Brown Niagaran reef belts would allow for subaerial exposure for extensive areas in the basin.

Deposition of carbonate sediment would occur with relative rises in sea-level and deposition of evaporites would occur with sea-level falls. Erosional surfaces, mudcracks, and imbricated grains observed throughout the cores suggest that the A-2 Carbonate sediments located in southwest Michigan experienced relatively high energy erosion and exposure at times and were likely near the intertidal and supratidal zones. The exposed sediments were likely influenced by sea-spray and storms that could bring in oceanic water to a normally dry environment. The A-2 Carbonate cores observed in this study were likely deposited in the same tidal flat environment that was defined by the basin margin and Brown Niagaran reef belt in southern Michigan. However, the deposits at each individual core location likely underwent exclusive, local rates of sediment supply, tidal influences and storm deposits that were dependent on the geometry of the tidal flat (Wright, 1984). The decussate texture observed in the PRINS core are consistent with the decussate texture observed in microbial mats in Gardner (1974). Butler (1969) states that the algal mats form among some of the hottest sites in the world and that temperatures and salinity are not limiting factors for formation in sabkha environments. Although, the A-2 Carbonate observed in this study resembles the Richfield Dolomite, complete cores are needed to propose a depositional sequence that is correlative for the A-2 Carbonate in southwest Michigan.

Stylolites of varying magnitude, class, and orientation occur throughout all the cores observed in this study indicating diffusive mass transfer throughout the A-2 Carbonate. Although horizontal stylolites are common in carbonate rock, the inclined and vertical oriented and the interconnected networks of stylolites suggest that tectonic activity affected the A-2 Carbonate. Reactivation of basement faults from the failed Fort Wayne rift or the Alleghanian Orogeny could provide the stress regime needed to generate non-bedding parallel stylolites.

The natural fractures observed throughout the A-2 Carbonate vary in the four cores used in this study. The fractures are nearly vertical in all of the cores, but the cement filling and openness of the fractures varies depending on the well locations. The cores from the V. Rabbers and H. Schaap wells have fractures that are completely open when compared to the anhydrite filled fractures in the cores from the S-503 and PRINS well. The vertical fracturing of the A-2 Carbonate likely occurred from shear stress acting parallel to the fracture plane from tectonic forces, post stylolitization. The fractures and stylolites may have a significant component of strike-slip motion from a compressional tectonic event, such as the Alleghanian Orogeny. However, subsidence resulting from underlying A-1 Evaporite salt dissolution and collapse may have created normal faults that have conjugate fracture networks or damage zones from shearing forces adjacent to the larger fault. Large faults located at the reported structural lineaments could propagate conjugate fractures in damage zones located in the natural gas producing A-2 Carbonate fields.

Nodular anhydrite and anhydrite laths are common throughout all the cores observed in this study. The carbonate mud around the nodules of anhydrite are often displaced and compacted indicating gypsum to anhydrite alteration prior to lithification. The anhydrite laths and decussate texture are commonly spread throughout the cores and along fractures but show no signs of displacing the carbonate mud, suggesting formation subsequent to lithification. The laths likely formed in the open pores of the A-2 Carbonate and along fractures. This resulted in the destruction of porosity and permeability in the A-2 Carbonate, especially in the S-503 and PRINS cores.

Overisel Reservoir Characterization

The characterization of the Overisel reservoir takes into account the geometric and structural interpretation of the A-2 Carbonate, petrophysical porosity and permeability values from rock cores, permeability estimates from OFPT data, gas flow rate data, and pre- and post-stimulation production data. The porosity values throughout the Overisel reservoir suggest that the A-2 Carbonate is a viable reservoir for natural gas storage, but the average core permeability value of 1.1 mD indicates a tight reservoir. The 3D static reservoir model illustrates several zones of higher porosity and permeability that are more favorable for gas storage and recovery. The A2D1 and A2D2 lithofacies (located adjacent to the A2A2 anhydrite lithofacies) and the interval within the A2D3 lithofacies have permeabilities and porosities above 5.0 mD and 15%. The three zones could be highly fractured intervals that are correlative throughout the Overisel field. Extensive borehole geophysical surveys using micro-resistivity and acoustic methods would be needed to further confirm the presence of fractures in these intervals. Alternatively, these zones could also be interpreted as facies similar to the dolomicrite that is present in core and thin sections that has abundant intercrystalline porosity and much larger, euhedral dolomite rhombs that likely has relatively higher permeability.

The higher permeability and porosity zones of 5.0 mD and 15% expire as elevation of the A-2 Carbonate decreases. This is consistent with the highest test average and absolute open hole flow rates of 1,800 Mcf/day and 40,000 Mcf/day measured in wells located on the structural highs of the Overisel reservoir. The A-2 Carbonate in the higher structures at the Overisel field could more closely resemble the reservoir lithofacies in the cores from the V. Rabbers and H. Schaap wells that have large open fractures and abundant vuggy porosity, rather than the tight dolomite represented throughout the S-503 core and most of the PRINS core. Without any core

samples from the Overisel field it is hard to speculate on the textures present based on comparisons with the observations made on cores from other fields.

Calculation of the OFPT permeability from pre-stimulation multi-rate open-flow potential well test data resulted in permeability values that are on average five times greater than the core analysis permeability values. The greater permeabilities can be attributed to either long-range correlation in vuggy porosity or fractures. However, the low average permeability value of 1.3 mD obtained from the core analysis is expected to be higher if vuggy porosity is the main factor in permeability estimates. Therefore, it is likely that fracture permeability enhances the Overisel reservoir, but it is unknown if these fractures only enhance permeability at the near-well scale or form larger networks that influence permeability at the reservoir-scale.

Based on comparisons of initial production with post stimulation production, acidizing and hydraulic fracturing of the A-2 Carbonate leads to increases in natural gas deliverability of natural gas exceeding 2300%. This dramatic increase in post-stimulation production may indicate that isolated fractures within the A-2 Carbonate are connected post treatment. Regardless, almost every well with available data experienced a considerable increase in production, suggesting that the A-2 Carbonate dolomite is a tight reservoir until the rock is acidized or hydraulically fractured.

Conclusions

The objective of this work was to explore the structural and stratigraphic controls on the deposition and diagenesis of the A-2 Carbonate in southwest Michigan with a focus on the Overisel gas storage reservoir. This study uses 3D static reservoir modeling from core analysis data, core and thin section observations from wells nearby, production and well test flow data,

and calculation of OFPT permeability from multi-rate open-flow well test data to characterize the Overisel reservoir. The work presented represents a framework that allows for the use of legacy data to re-interpret and re-analyze older natural gas producing fields. This approach could have applications for gas and oil field conversion/re-purposing such as gas storage and secondary recovery. With the data presented several inferences can be made.

(i) Structure of the A-2 Carbonate producing fields in southwest Michigan is likely from a combination of basement features and dissolution of the surrounding A-1 Salt.

(ii) The observations in core and thin sections suggests that the A-2 Carbonate formed in an arid tidal flat, sabkha environment and that subsequent diagenesis varied on a regional scale.

(iii) Porosity is fairly consistent and is normally distributed throughout the Overisel reservoir. Permeability values are relatively low throughout the reservoir and lognormally distributed.

(iv) The 3D static reservoir model indicates three zones in the structurally higher parts of the Overisel reservoir with higher porosity and permeability values.

(v) Permeability from core analysis is considerably lower than the OFPT permeability suggesting enhanced permeability by fractures.

(vi) The production data, absolute open hole flow, and test flow averages show that the structurally higher parts of the reservoir are the most productive.

(vii) Hydraulic fracturing and acidizing are key components of reservoir production.

CHAPTER III

GENERAL CONCLUSIONS AND FUTURE WORK

The objective of this work was to explore the structural, depositional, and diagenetic controls of the A-2 Carbonate in southwest Michigan with a focus on the Overisel gas storage reservoir. Characterization of the Overisel reservoir occurred through 3D static reservoir modeling from core analysis data, core and thin section observations from nearby wells, production and well test flow data, and calculation of OFPT permeability from multi-rate open-flow well test data. Subsurface mapping using gamma-ray and neutron wire-line logs suggests the structure of the A-2 Carbonate producing fields in southwest Michigan is likely from a combination of Pre-Cambrian basement features and dissolution of the surrounding A-1 Salt. The observations in core and thin sections suggests that the A-2 Carbonate formed in an arid tidal flat, sabkha environment and that subsequent diagenesis varied on a regional scale. Core porosity is fairly consistent and is normally distributed throughout the Overisel reservoir. Permeability values measured from cores are relatively low throughout the reservoir and lognormally distributed. The 3D static reservoir model generated from core permeability and porosity indicates three zones in the structurally higher regions of the Overisel reservoir with higher porosity and permeability values. Core permeability values are considerably lower than OFPT permeability suggesting enhanced fracture permeability in the Overisel reservoir. The production data, absolute open hole flow, and test flow averages show that the structurally higher regions of the Overisel reservoir are the most productive. Pre- and post-stimulation production data indicate that hydraulic fracturing and acidizing are key components of reservoir production.

The accuracy of the interpretations and findings of this study are limited to available data. The acquisition of additional datasets would greatly enhance this work and further explore the

characterization of the A-2 Carbonate in southwest Michigan. Acquisition of a 3D seismic survey would confirm the presence of the A-1 Salt around the A-2 Carbonate fields, and the survey could also confirm and the distinguish the extent of larger faults and underlying Pre-Cambrian basement features. Drilling and core retrieval within deeper wells would confirm the presence of the A-1 Salt and provide data to observe the textures of the A-2 Carbonate and other Silurian formations. Testing the mechanical properties of the core, such as Young's modulus, would be helpful for understanding if the enhanced porosity and permeability in the static 3D reservoir model can be attributed to matrix porosity and permeability or fractures. Running oriented circumferential borehole image logs in new wells or wells that have not been acidized or hydraulically fractured would allow for the necessary data to generate a fracture network model for better prediction of fracture impacts on permeability and fracture network geometry.

APPENDIX A
Core/Thin Section Photographs and Observations

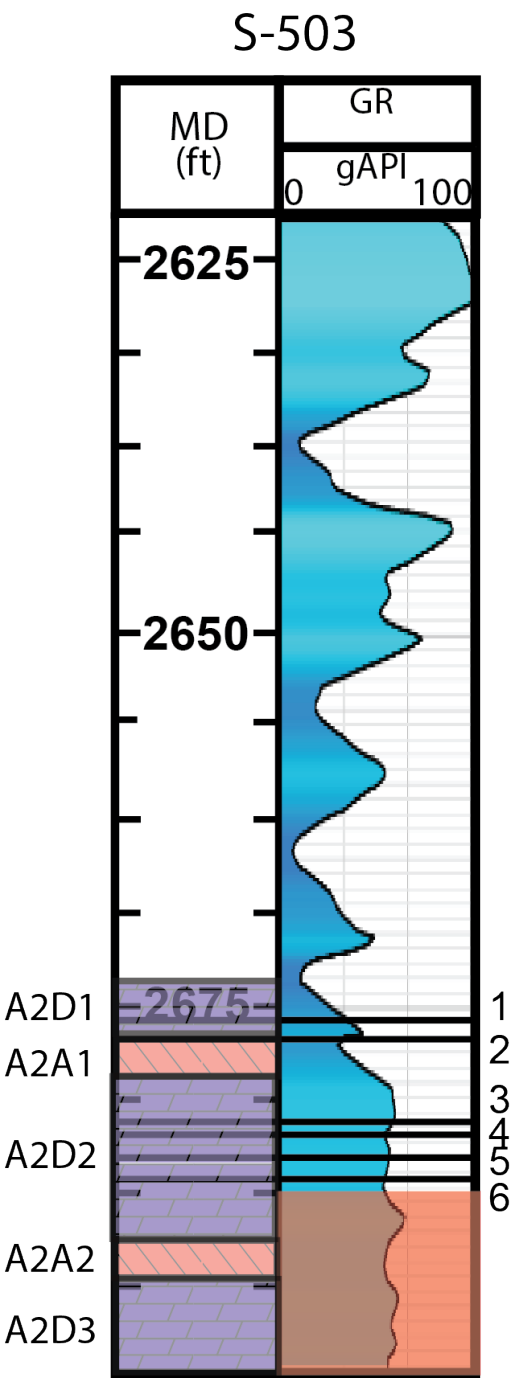

Figure A-1. The gamma-ray log for the S-503 gas observation well located in the Salem gas storage field. The depths of the defined lithofacies in the study are located on the left of the log. The red portions covering the gamma-ray signature indicate core that is unavailable for observation.

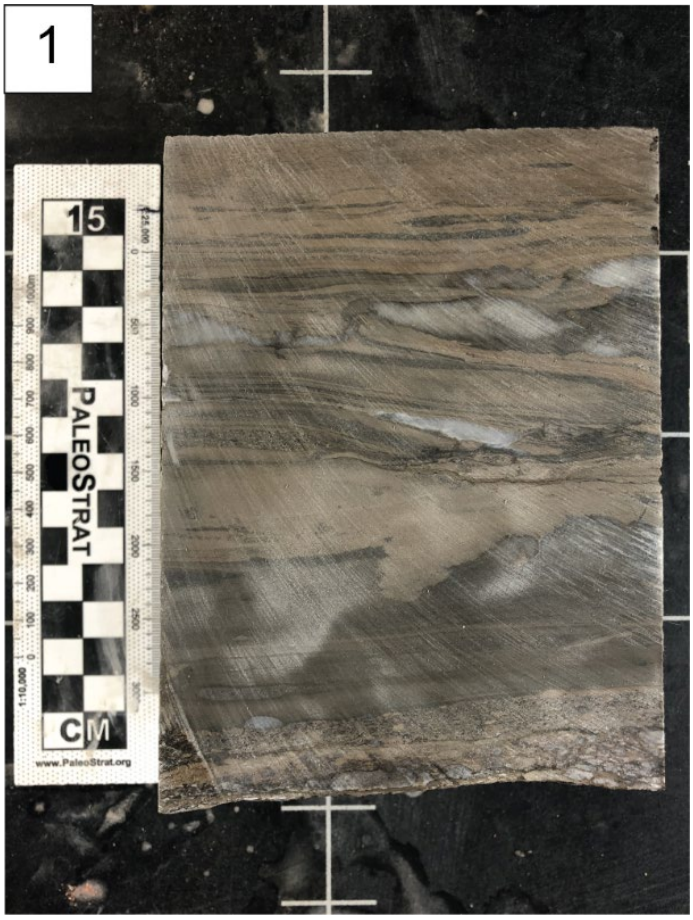

Figure A-2. Dolomicrite with an dolowackestone layer near the bottom. Compacted nodular anhydrite inclusions and erosional surfaces are present. The oolitic layer contains rounded to sub-rounded, carbonate clasts and anhydrite nodules. Stylolite development occurs between the dark and light dolomicrite beds.

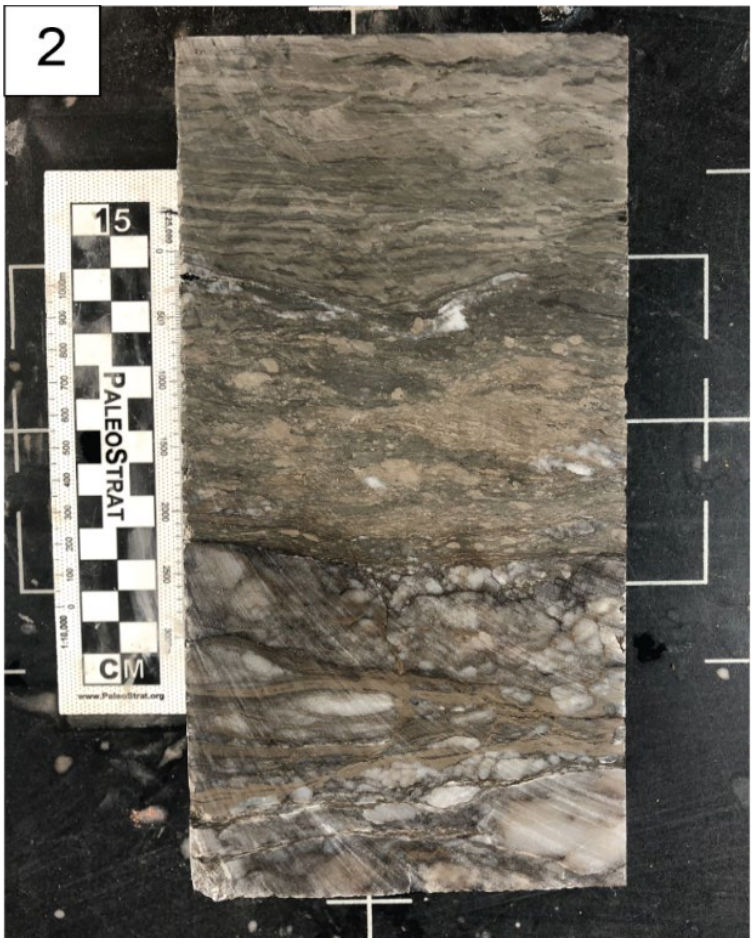

Figure A-3. Laminated dolowackestone with subrounded grains. Compacted and elongated nodular anhydrite within the dolowackestone. Chicken wire anhydrite with dolomite stringers is present at the bottom of the sample. Horizontal stylolites are present throughout the sample.

Figure A-4. Laminated dolomicrite with possible desiccation fractures. Dense anhydrite bed is at the bottom of the sample. Horizontal stylolites are common in the sample. Multiple erosional surfaces present with fractures that are mostly filled with anhydrite throughout the sample.

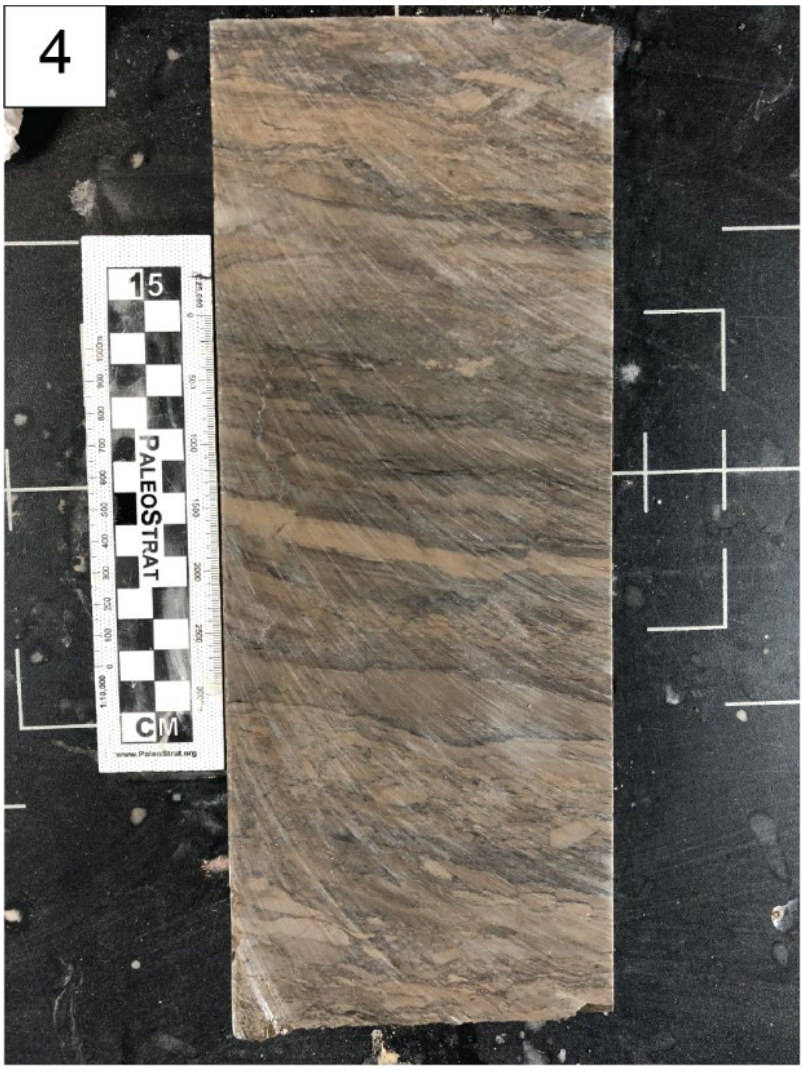

Figure A-5. Dolomicrite and dolopackstone with abundant stylolitzation. Grains are sub-rounded, elongated and imbricated. Beds are offset from vertical fractures.

Figure A-6. Laminated dolomicrite with large, compacted nodular anhydrite inclusions parallel to bedding. Vertical fractures are present in the dolomicrite.

Figure A-7. Dolomicrite with large nodular anhydrite inclusions. Horizontal and inclined stylolites are present. Small, dark anhydrite laths are spread throughout the sample.

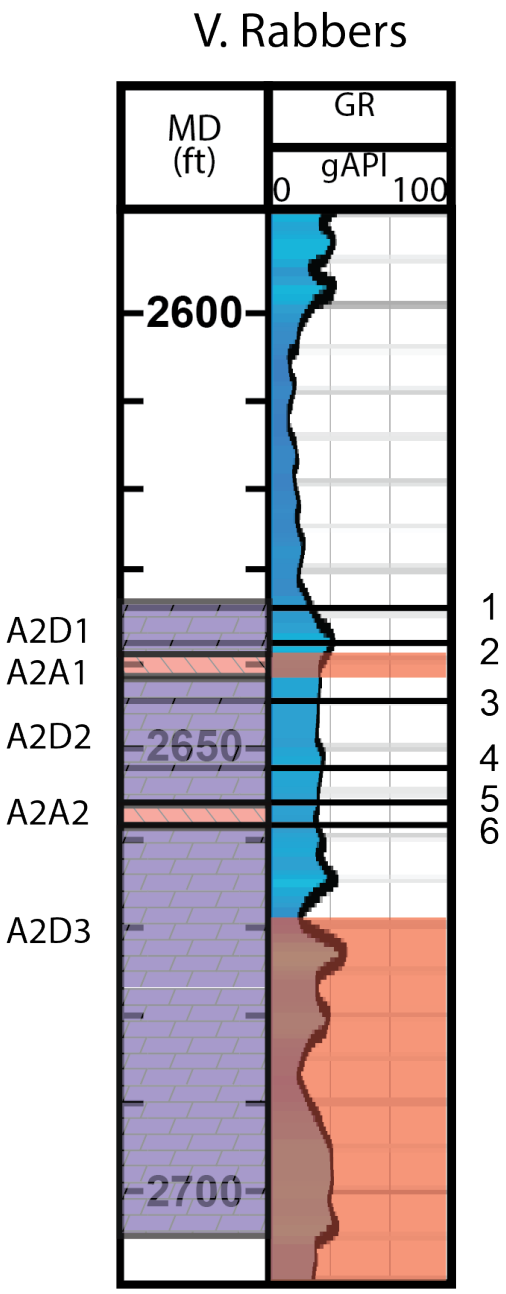

Figure A-8. The gamma-ray log for the V. Rabbers gas producing well located in the Fillmore gas producing field. The depths of the defined lithofacies in the study are located on the left of the log. The red portions covering the gamma-ray signature indicate core that is unavailable for observation.

Figure A-9. Dolomicrite with a small brecciated interval with anhydrite inclusions. Inclined and vertical stylolites are cross-cutting throughout the sample. Some of the stylolites contain anhydrite and pyrite inclusions. Vuggy porosity and open vertical fractures are present throughout the sample.

Figure A-10. Dolomicrite with abundant horizontal and inclined stylolites. Vertical fractures offset the horizontal stylolites. Vuggy porosity is present but mostly filled with anhydrite laths.

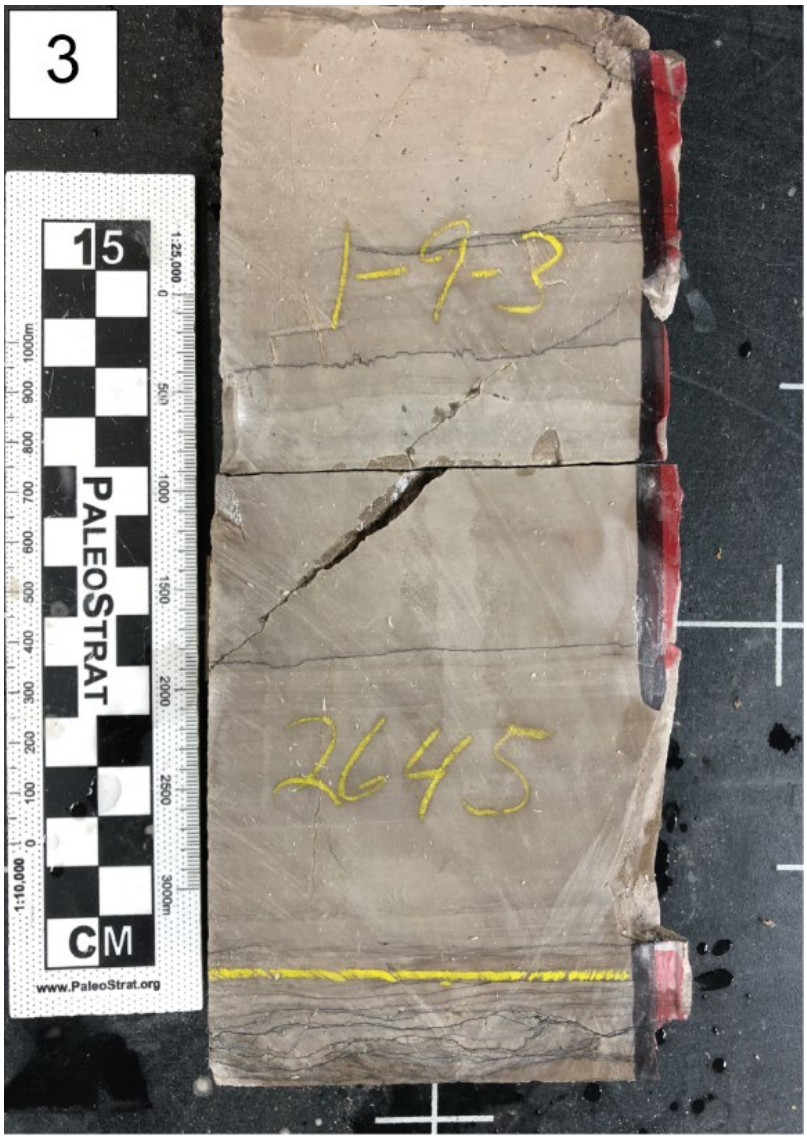

Figure A-11. Dense dolomicrite and laminated dolomicrite with open fractures. Horizontal and inclined stylolites are present throughout the sample.

Figure A-12. Laminated dolomicrite and dolowackestone with abundant vuggy porosity present throughout the sample. The sample is heavily oil stained and has sucrosic dolomite in the large open pores.

Figure A-13. Dolomicrite with a dolowackestone interval. Horizontal wavy and digitate stylolites are present. The dolowackestone clasts are sub-rounded. A highly disturbed bed with abundant anhydrite laths is present at the top of the sample.

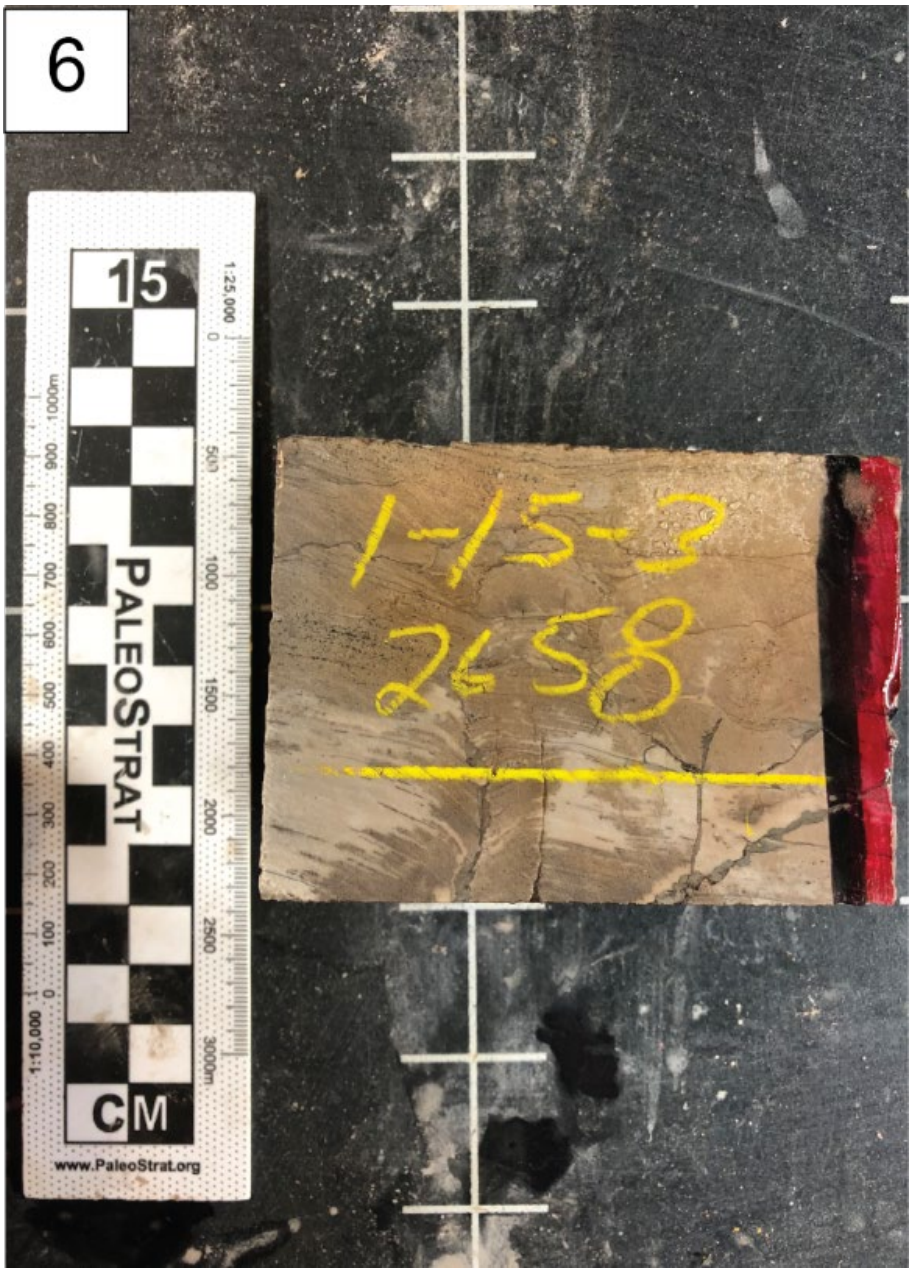

Figure A-14. Dolomicrite with open, vertical fractures cutting through a stromatoporoid fossil (?). Abundant horizontal and inclined stylolites are present in the sample.

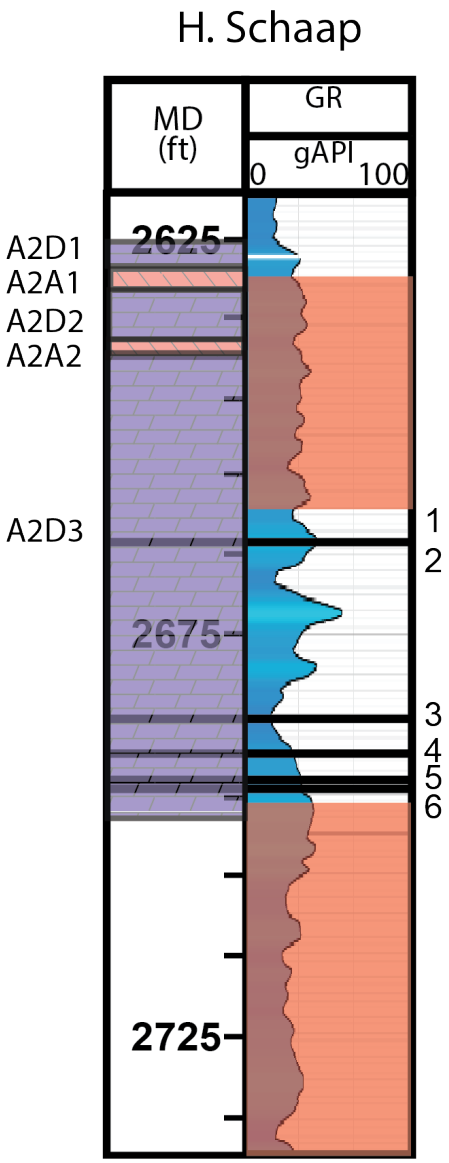

Figure A-15. The gamma-ray log for the H. Schaap gas producing well located in the Fillmore gas producing field. The depths of the defined lithofacies in the study are located on the left of the log. The red portions covering the gamma-ray signature indicate core that is unavailable for observation.

Figure A-16. Light dolomicrite with large vugs partially filled with sucrosic dolomite. Vertical fractures cut into the vugs. The sample is from the bottom of the natural gas pay zone.

Figure A-17. Dolorubblestone with varying grain size and shape. Abundant stylolites occur around the grains. Micro-vugs and anhydrite laths are spread throughout the sample.

Figure A-18. Dolomicrite with vertical and horizontal stylolites throughout the sample. Vertical fractures are present with some vuggy porosity. Lighter dolomite stringers are present throughout the sample. The fractures cut and offset the stylolites.

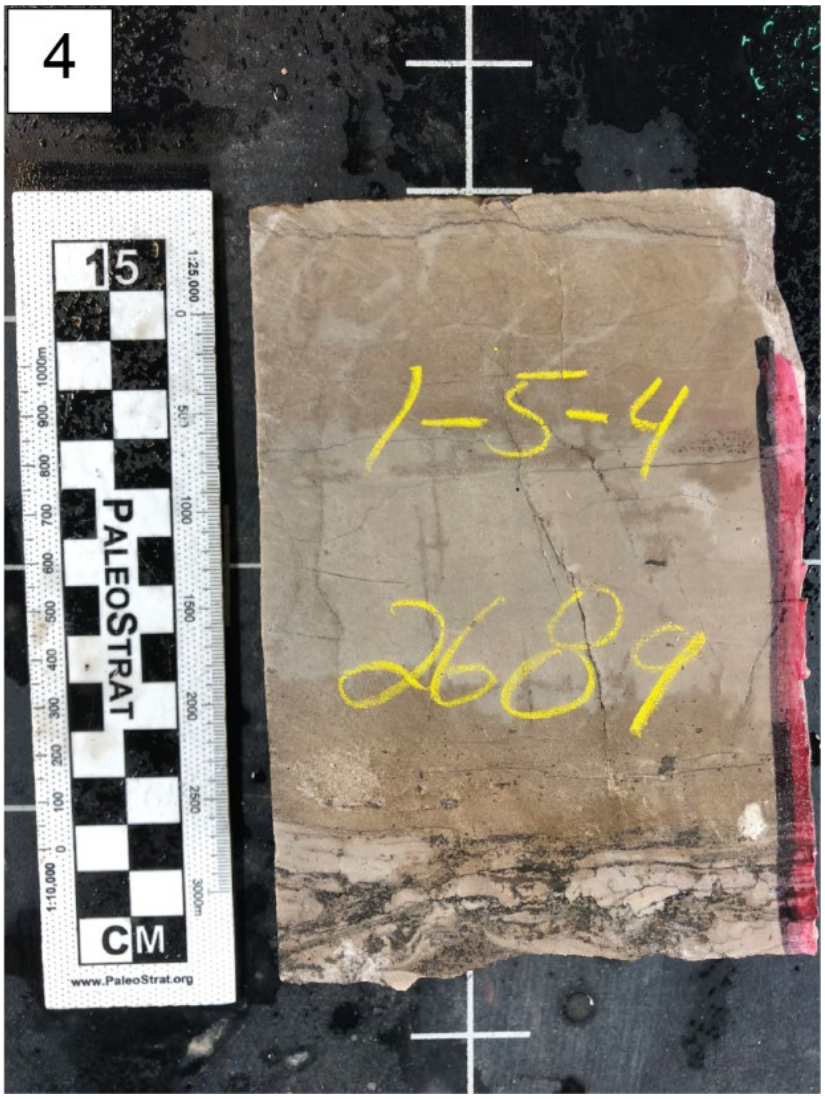

Figure A-19. Dolomicrite with a dolopackstone bed at the bottom of the sample. Open vertical fractures are present throughout the dolomicrite. The dolopackstone bed contains anhydrite laths that surround the lighter dolomite clasts. Clasts are angular and possibly imbricated.

Figure A-20. Dolomicrite with abundant vuggy porosity. Open, vertical fractures are present throughout the sample. Horizontal stylolites are common in the sample.

Figure A-21. Dolomicrite and dolorubblestone with interconnected vertical and horizontal stylolites that run throughout the sub-angular clasts. Vuggy porosity with sucrosic dolomite filling is present throughout the sample. Varying sized, open, vertical fractures cut across the stylolites.

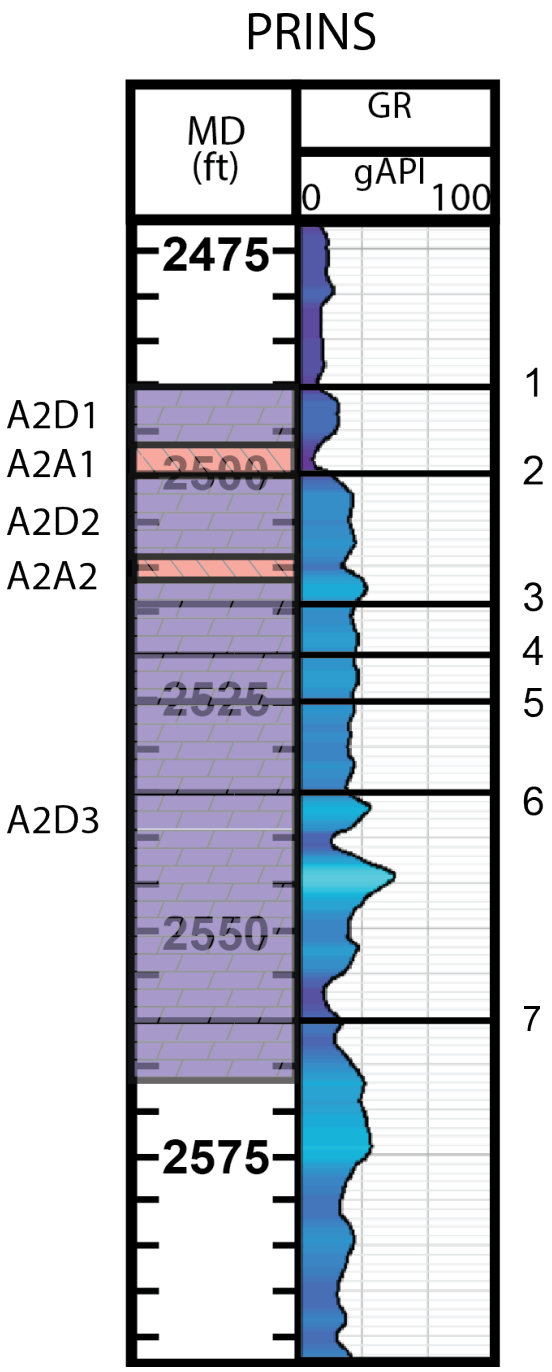

Figure A-22. The gamma-ray log for the PRINS dry hole well located 2 miles south of the Overisel gas storage field. The depths of the defined lithofacies in the study are located on the left of the log. The red portions covering the gamma-ray signature indicate core that is unavailable for observation.

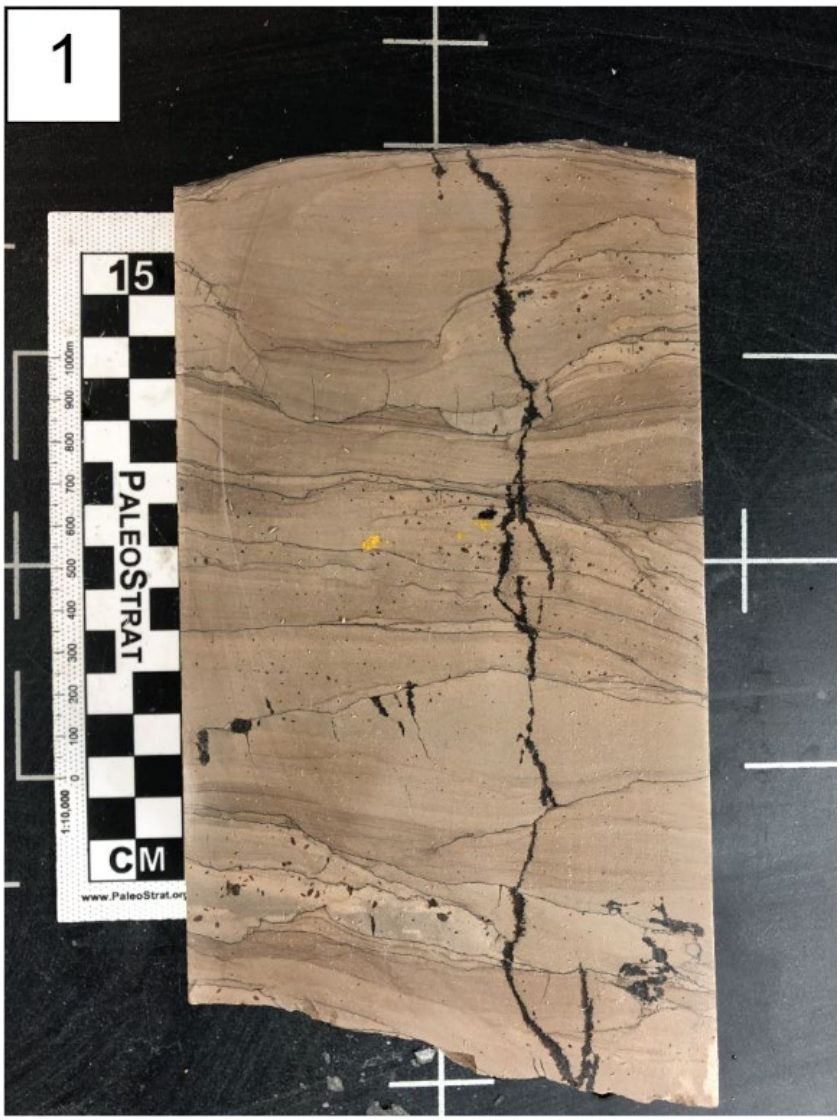

Figure A-23. Dolomicrite with abundant horizontal stylolites present. A vertical fracture filled with anhydrite laths cuts across the stylolites. Anhydrite laths are spread throughout the sample in the dolomicrite and along stylolites.

Figure A-24. Decussate texture within an algal mat (?) with coarse anhydrite laths spread throughout wavy dolomicrite. Horizontal stylolites are common throughout the sample.

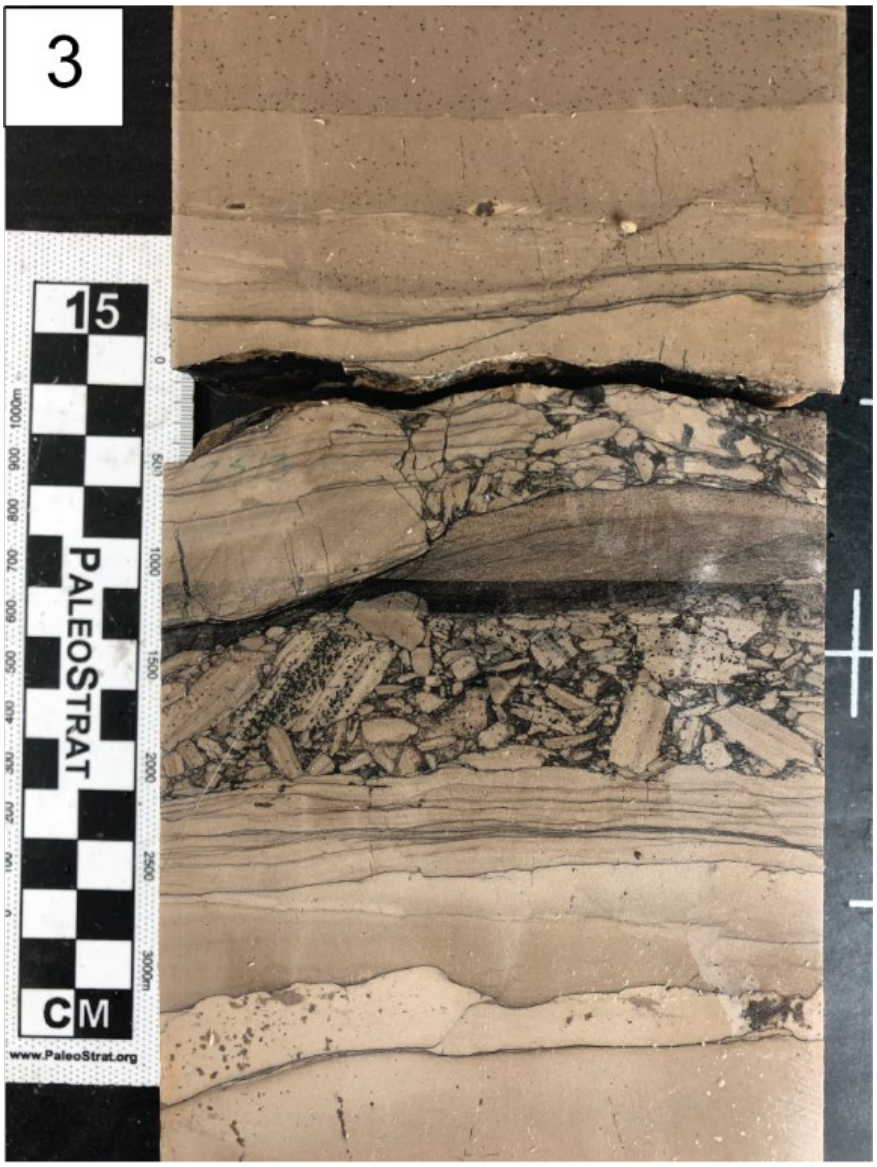

Figure A-25. Dolomicrite and grainstone. The clasts are large, angular, and appear imbricated. The clasts are surrounded with dark anhydrite laths. Horizontal stylolites and vertical fractures are present throughout the core.

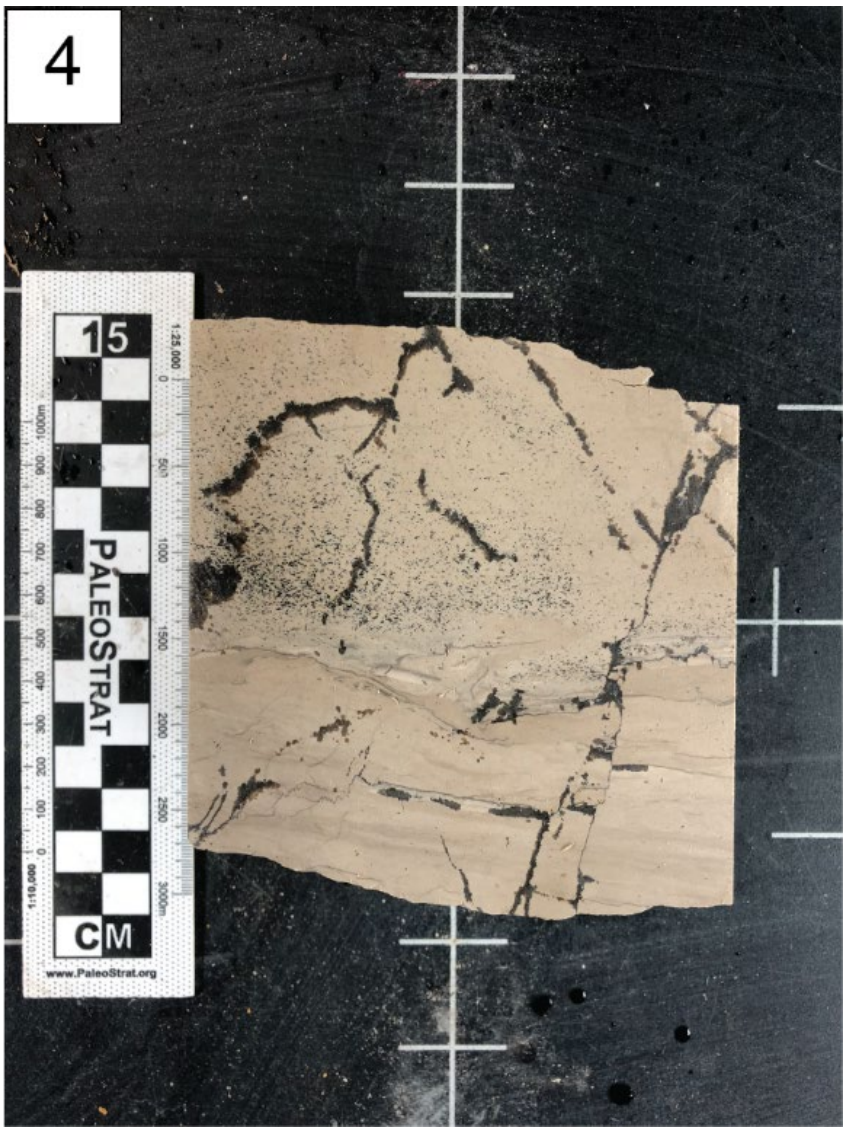

Figure A-26. Dolomicrite with large, vertical fractures. The fractures contain anhydrite laths and cut and offset horizontal stylolites and brecciated bed. The anhydrite laths are spread throughout the matrix of the dolomicrite.

Figure A-27. Soft sediment folding in dolomicrite with a dolowackestone bed at the top of the sample. The clasts in the dolowackestone are elongated and imbricated. Desiccation cracks are present near the bottom of the dolomicrite.

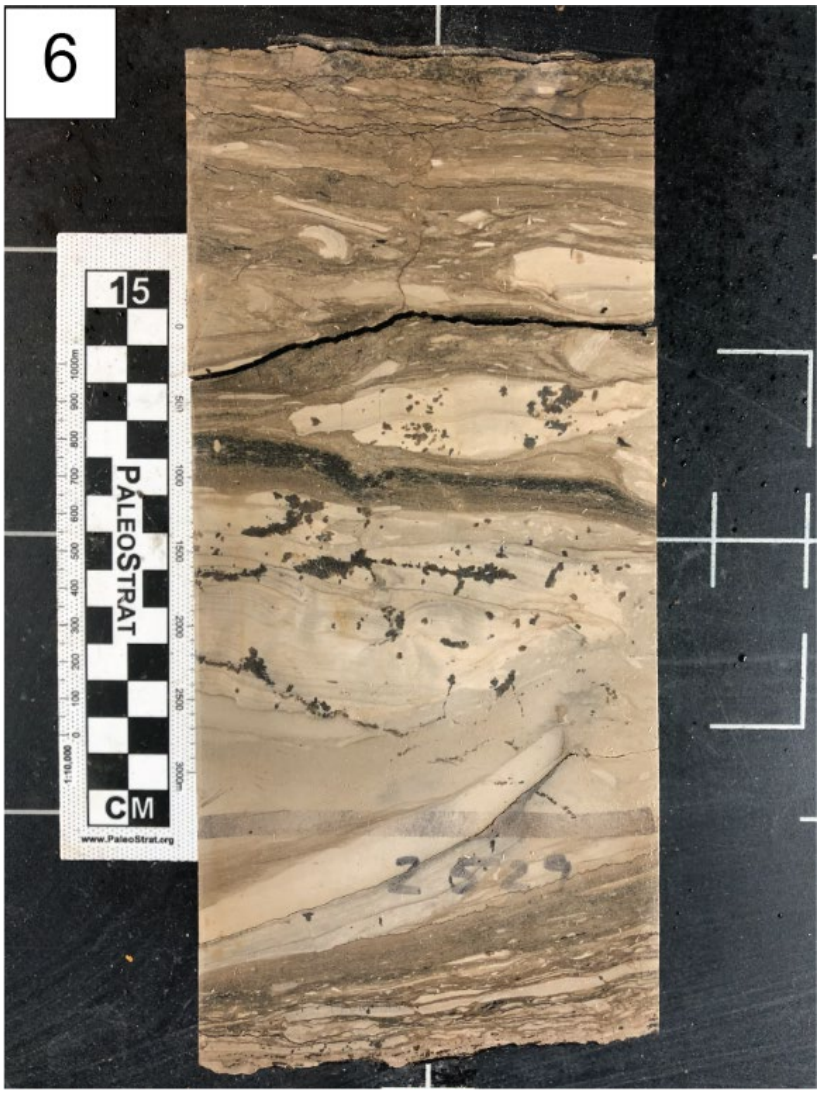

Figure A-28. Dolowackestone and dolopackstone with elongated and imbricated clasts. Soft sediment folding is present in the middle of the sample. Anhydrite laths are oriented and occupying select layers and features.

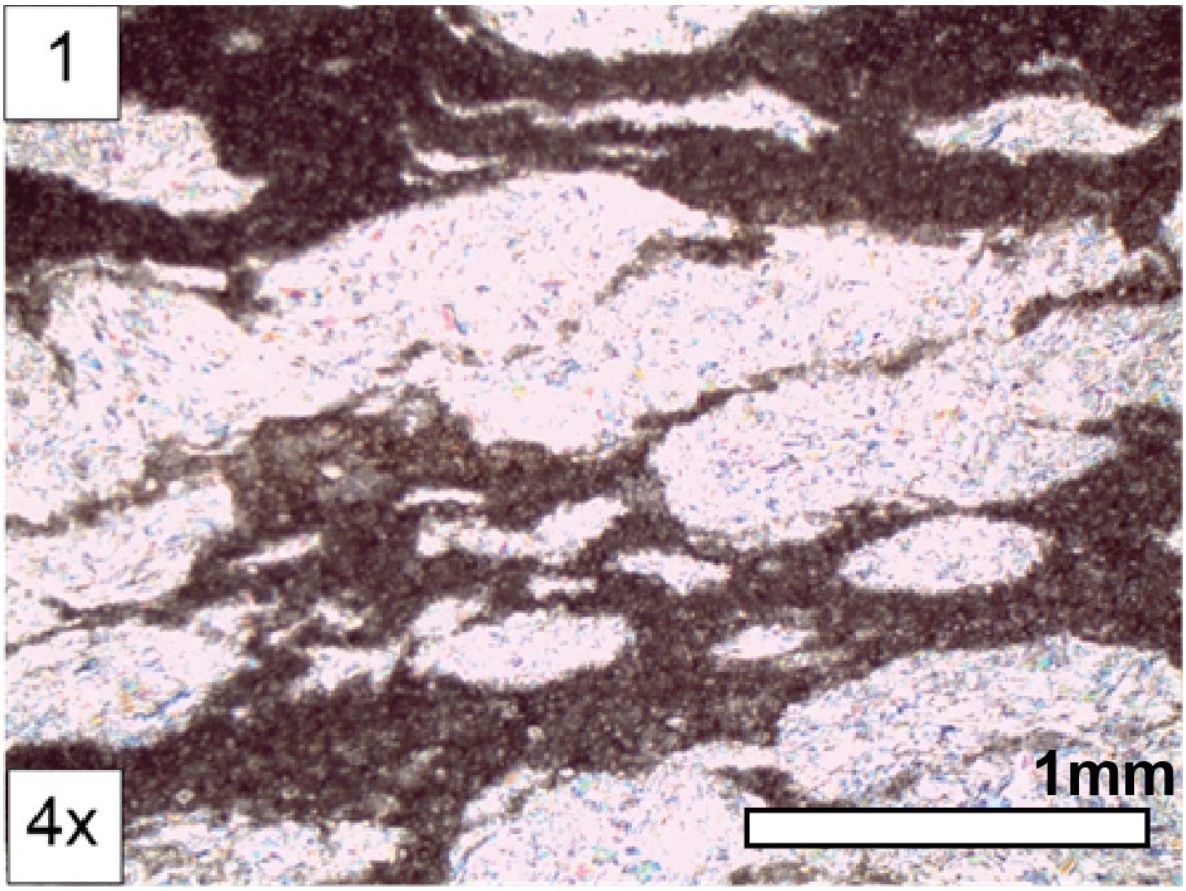

Figure A-29. Finely crystalline, micritic dolomite with nodular anhydrite present throughout. Larger subhedral dolomite rhombs are spread throughout the muddy matrix. The anhydrite nodules are elongated and appear compacted.

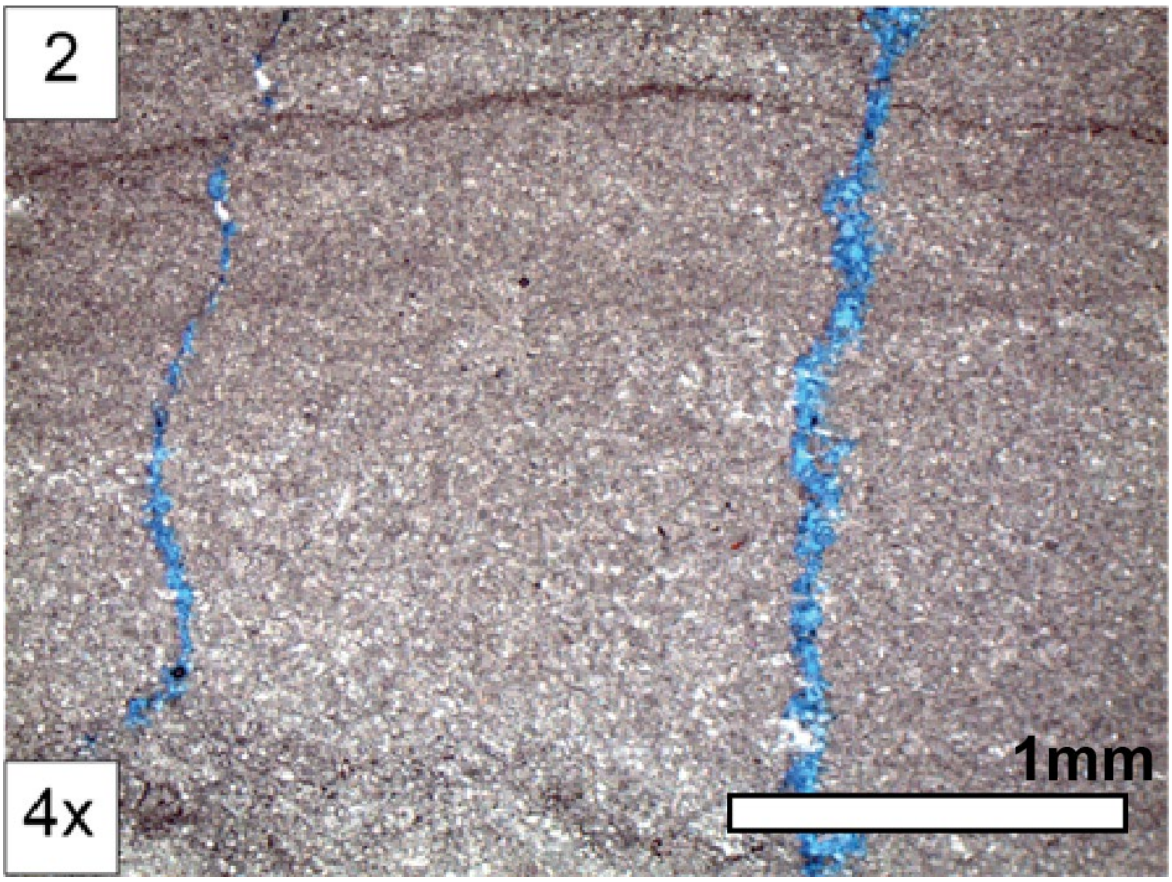

Figure A-30. Finely crystalline, micritic dolomite with larger, subhedral dolomite rhombs spread throughout the matrix. There are open, vertical fractures that cut across horizontal stylolites.

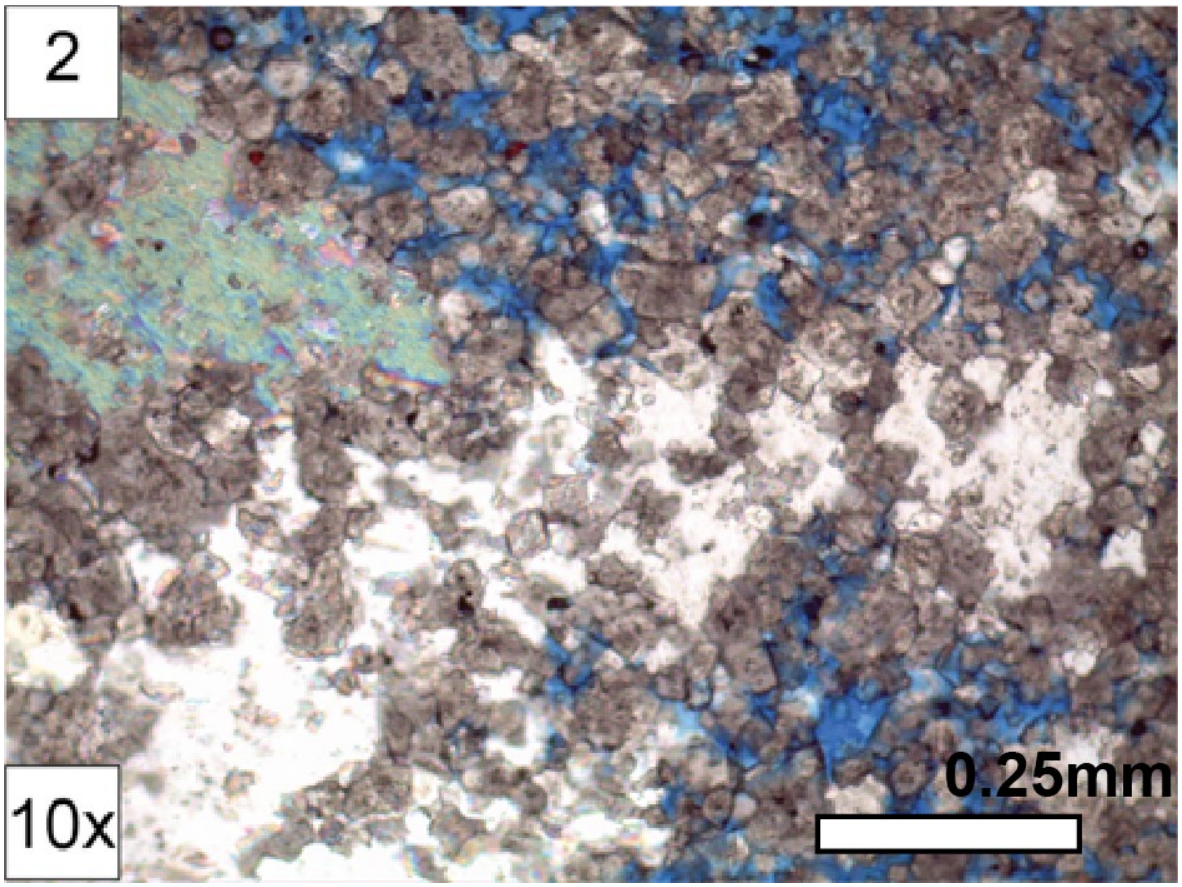

Figure A-31. Subhedral, planar dolomite rhombs with abundant porosity present. Anhydrite cement is shown filling the void space around the dolomite rhombs.

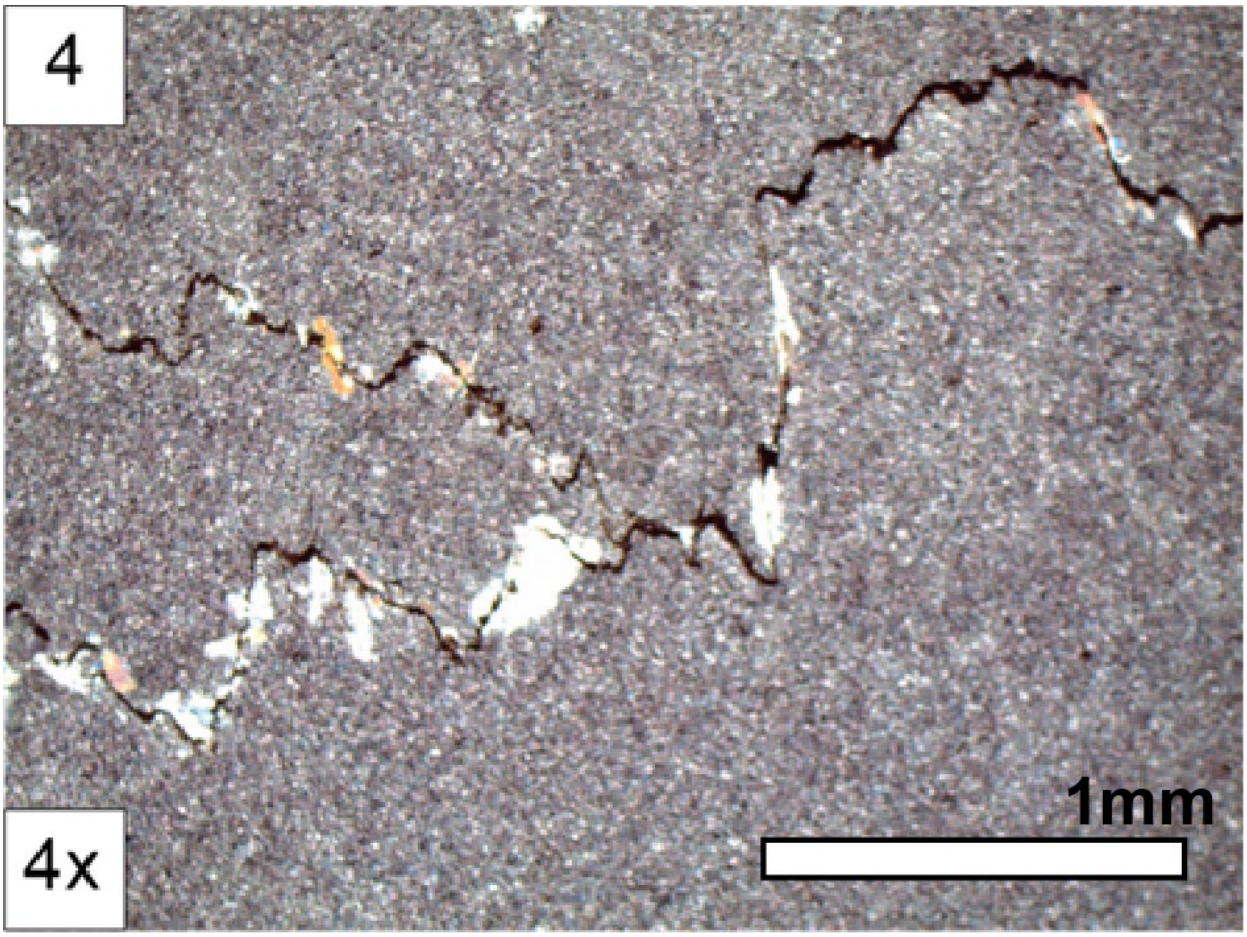

Figure A-32. Finely crystalline, micritic dolomite with horizontal stylolites present. Stylolites contain anhydrite nodules that are oriented with the stylolites.

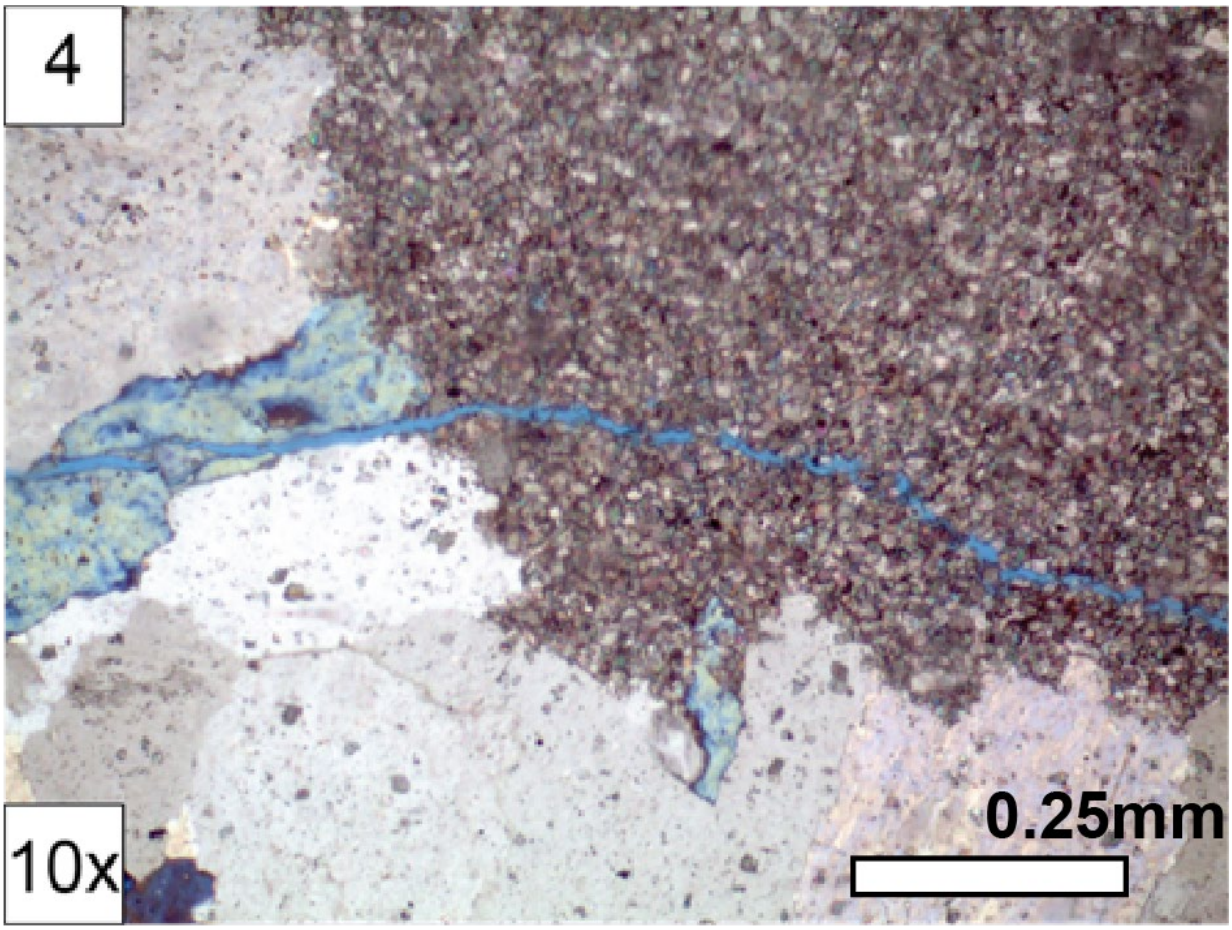

Figure A-33. Finely crystalline, micritic dolomite with large anhydrite nodules present throughout the sample. A horizontal, open fracture cuts across the dolomite matrix but terminates into the anhydrite nodule. Dolomite rhomb inclusions are present in the anhydrite.

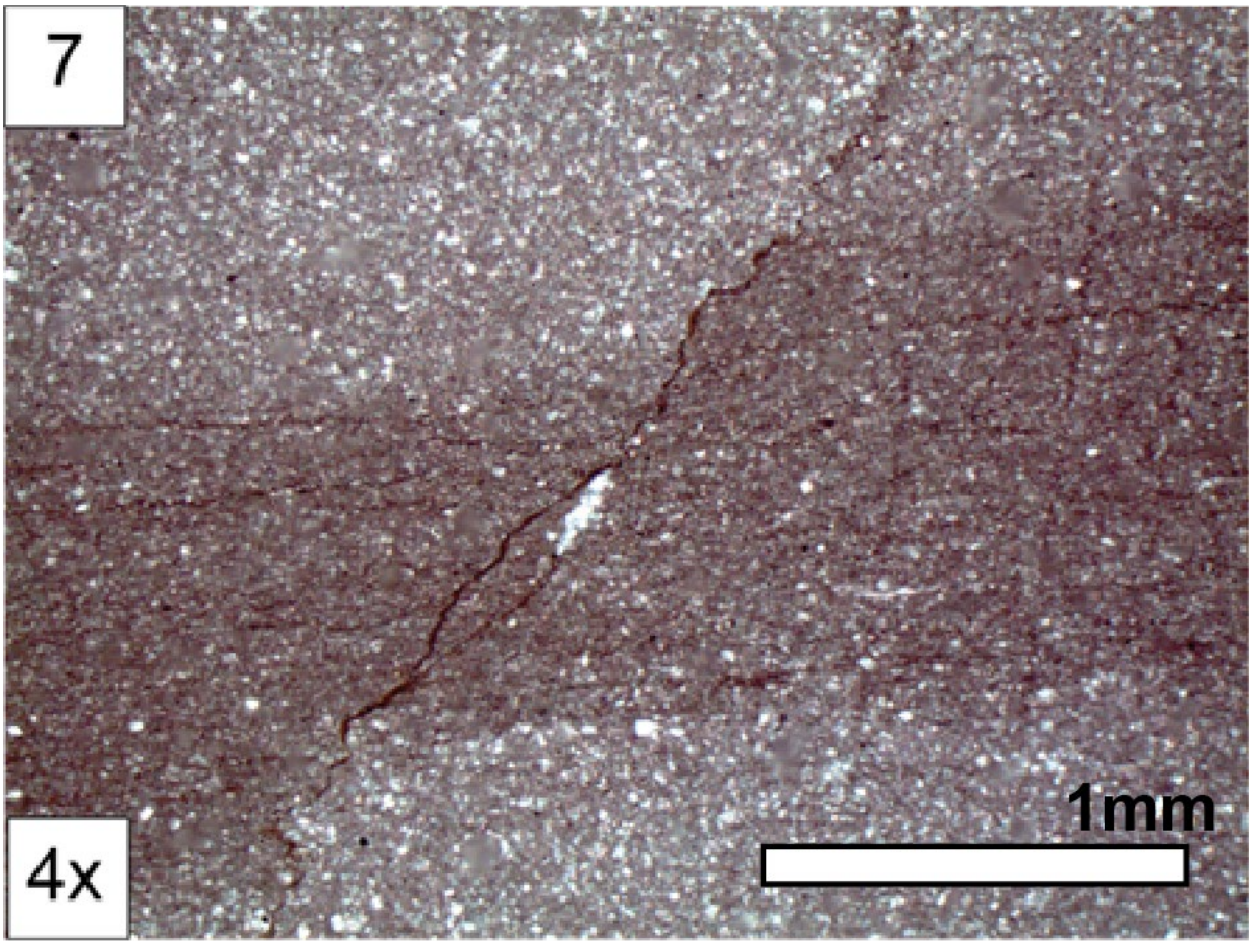

Figure A-34. Finely crystalline, micritic dolomite with larger dolomite rhombs spread throughout the matrix. Normal micro-fault offsets the darker micrite bed. Fracture is filled with darker, possibly organic rich material.

APPENDIX B
Core Analysis Plots

Appendix B

Permeability and porosity values were collected from core analysis from 77 wells in the Overisel gas storage field. The data was analyzed and organized into cross-plots, histograms, and probability plots for the entire A-2 Carbonate and for the subsequent lithofacies.

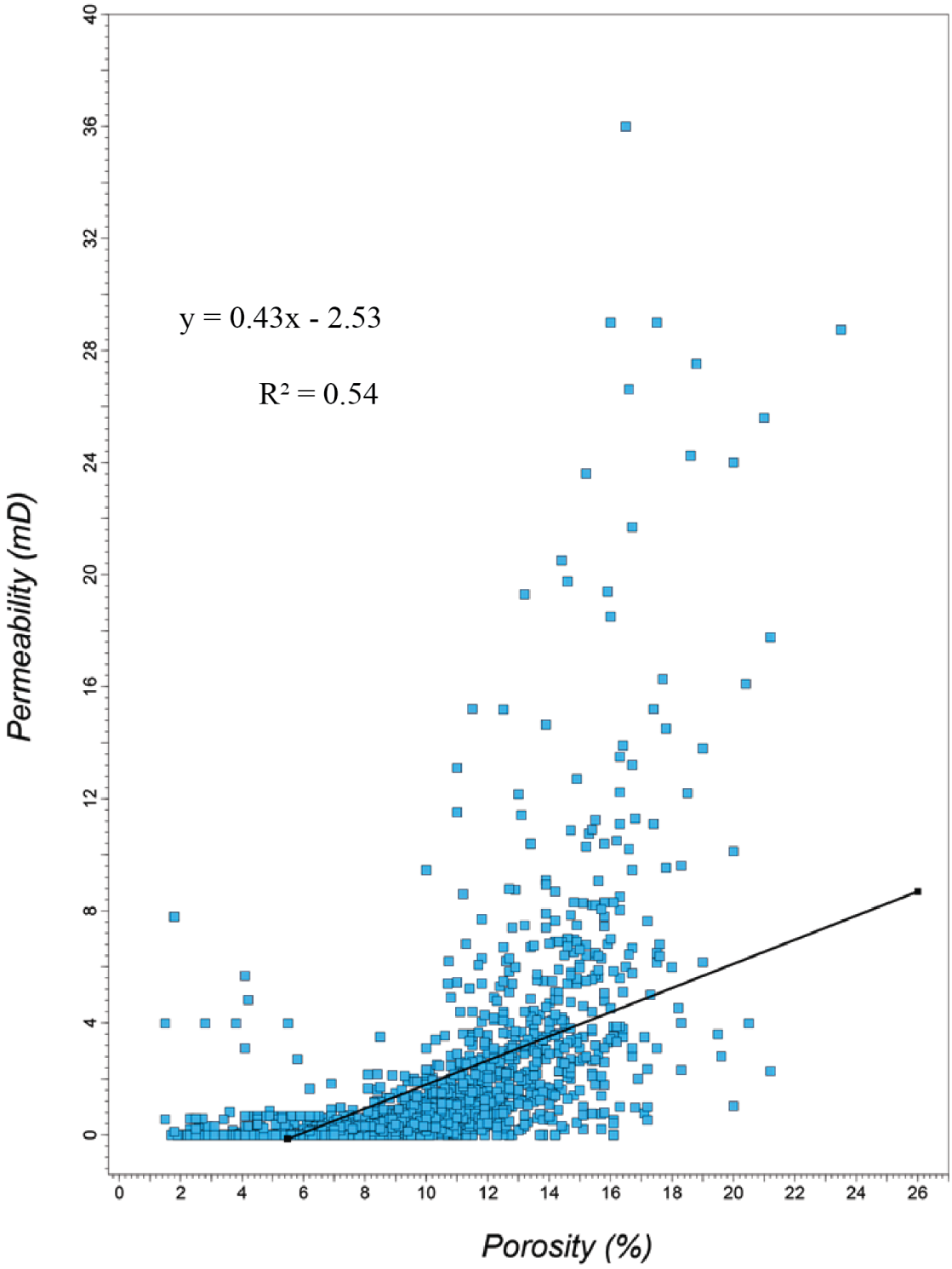

Figure B-1. Plot of permeability and porosity measurements from core analysis of 77 wells in the Overisel field. The linear regression line and equation with the coefficient of correlation are presented.

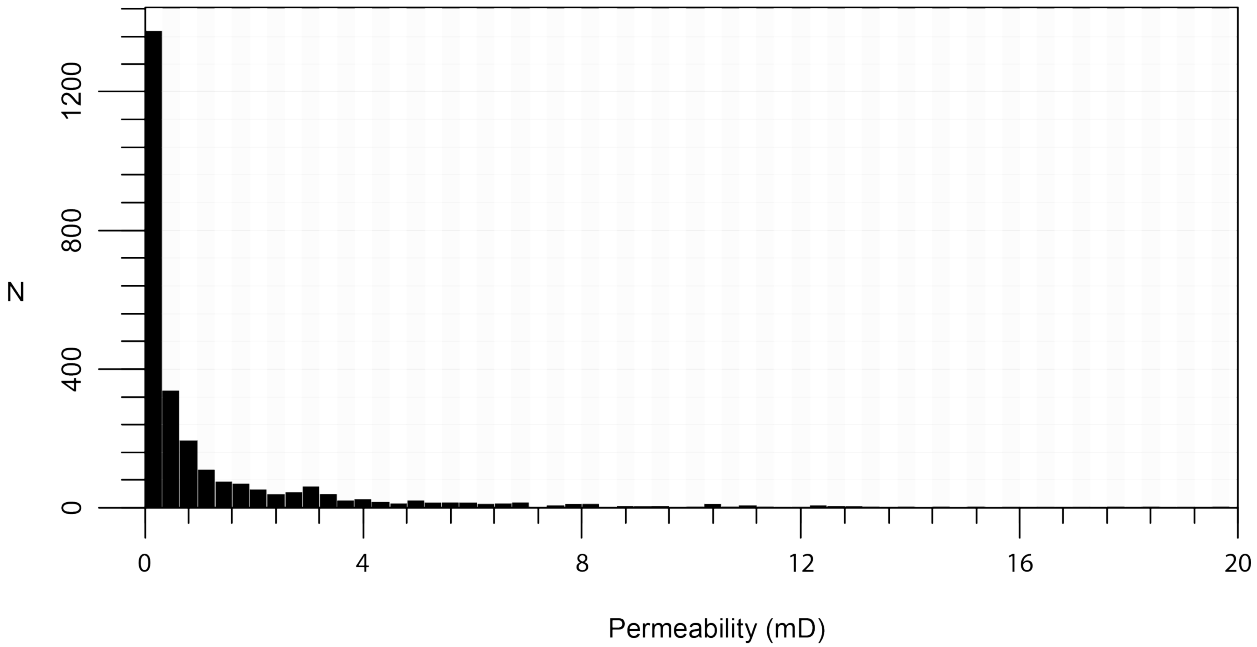

Figure B-2. Histogram of the permeability values measured from core analysis for all three reservoir lithofacies in the Overisel field.

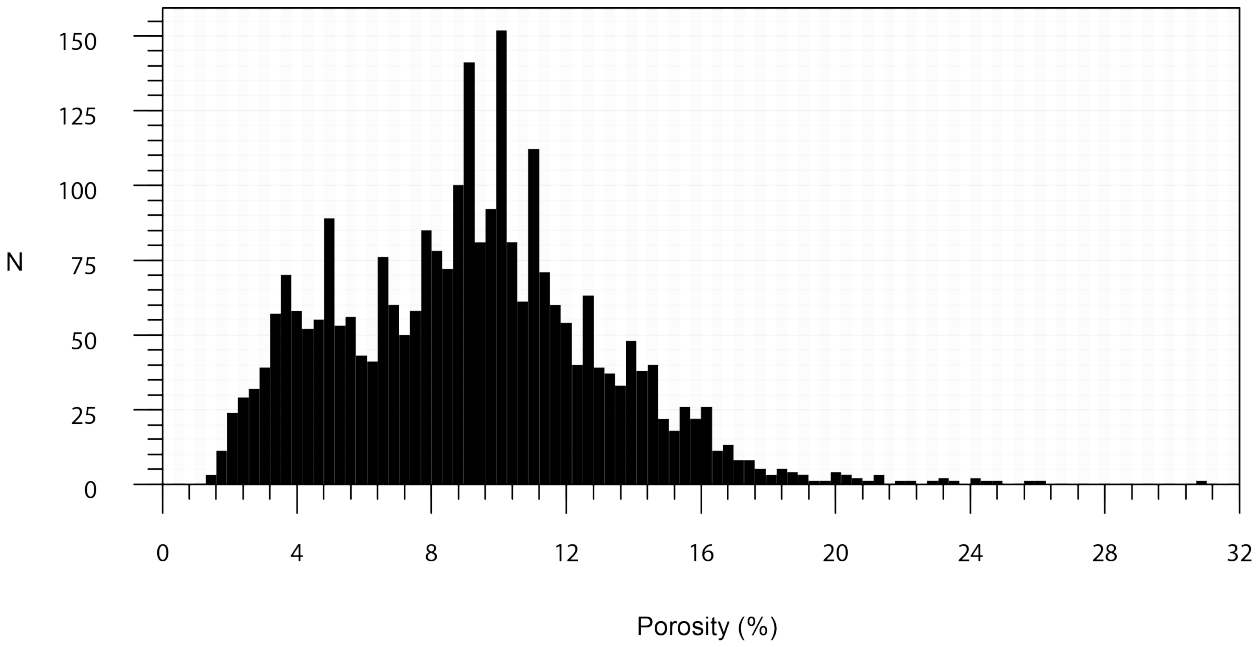

Figure B-3. Histogram of the porosity values measured from core analysis taken in the three reservoir lithofacies in the Overisel field.

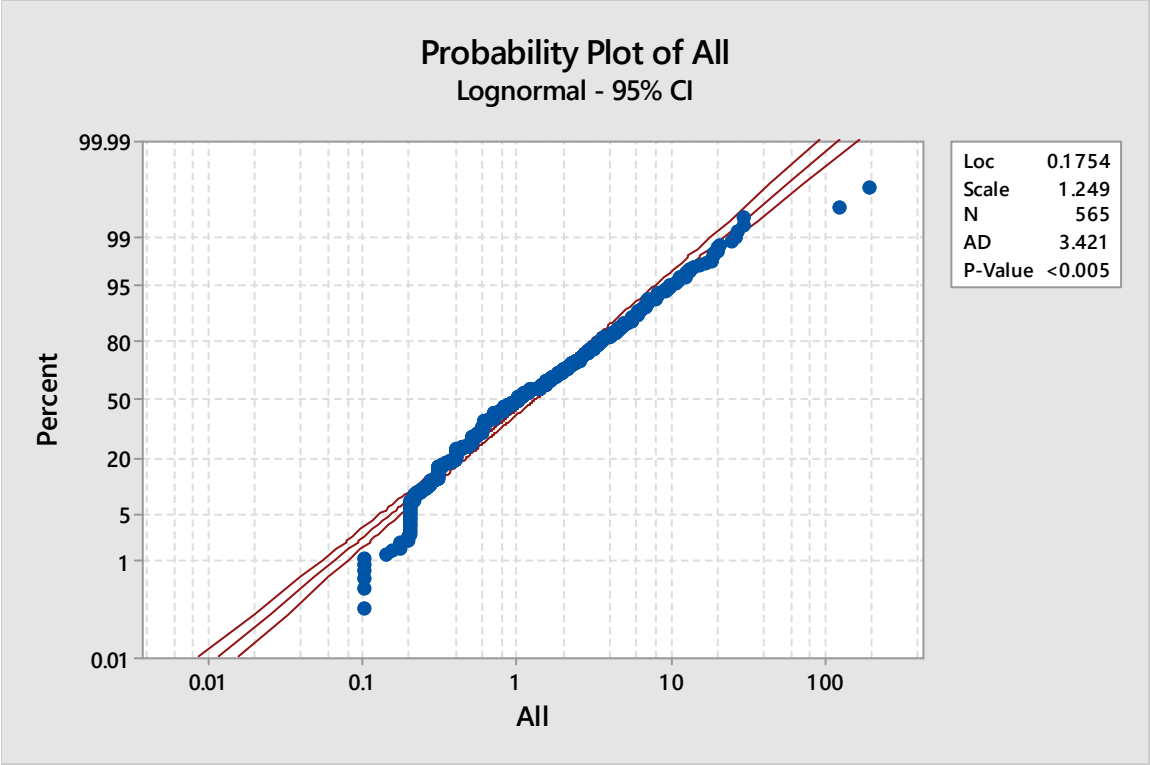

Figure B-4. Lognormal probability plot of A2D1 lithofacies permeability values. The curved lines present 95% confidence intervals.

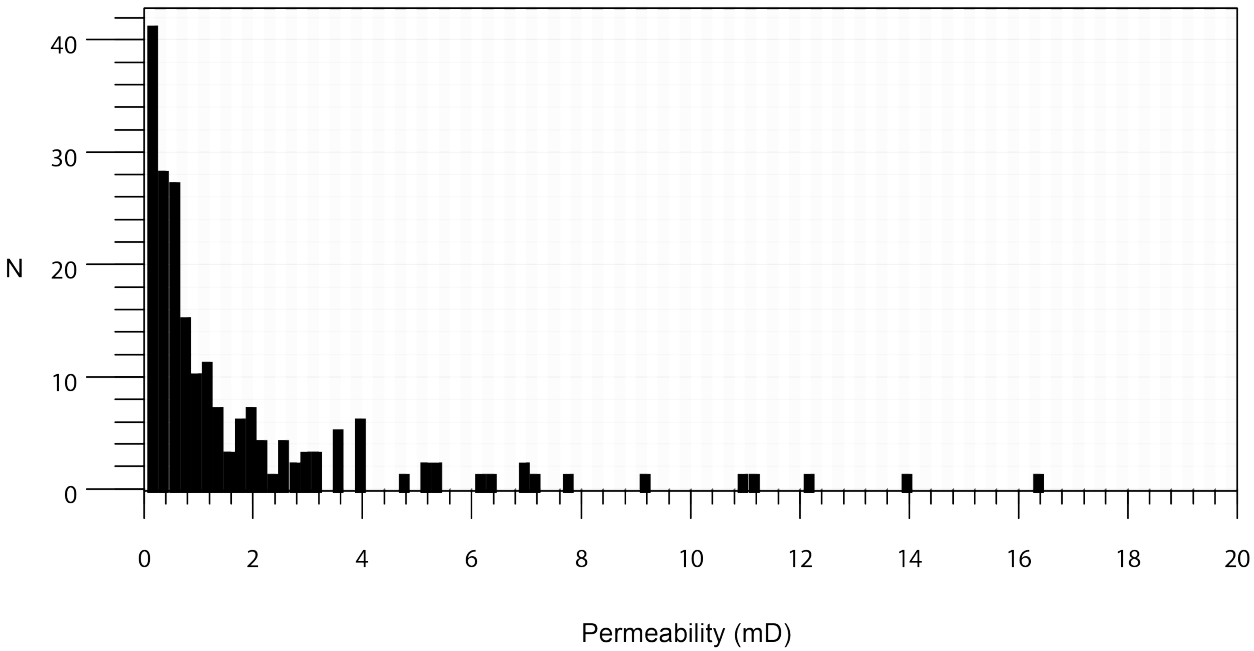

Figure B-5. Histogram of the permeability values measured from core analysis taken in the A2D1 lithofacies in the Overisel field.

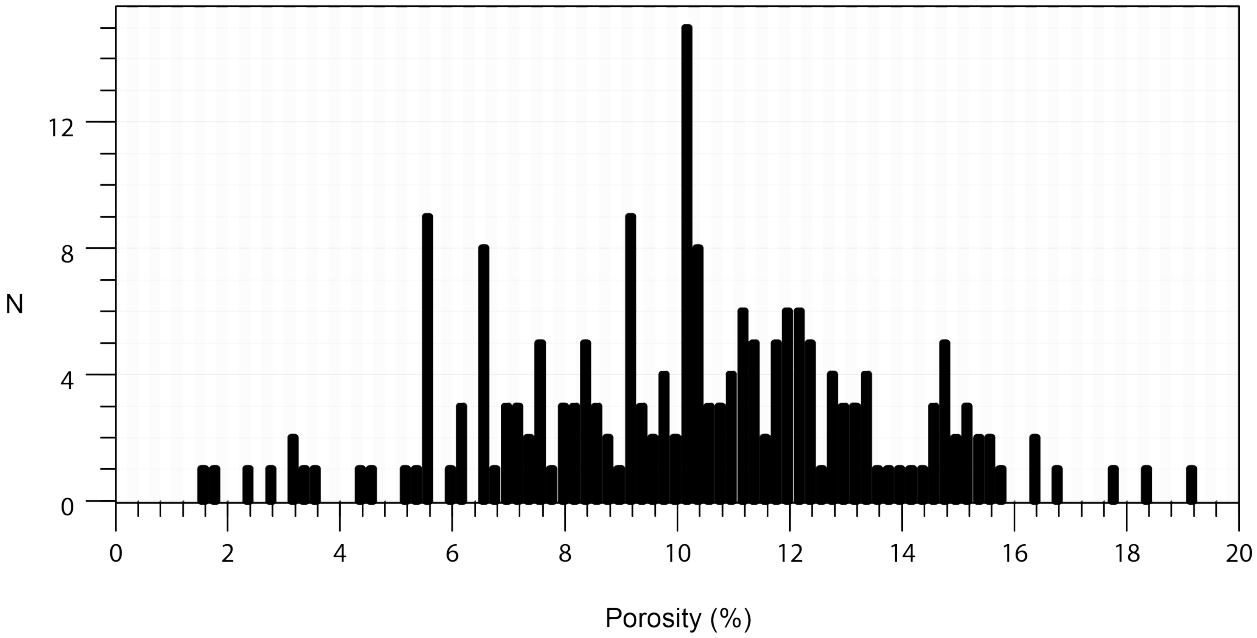

Figure B-6. Histogram of the porosity values measured from core analysis taken in the A2D1 lithofacies in the Overisel field.

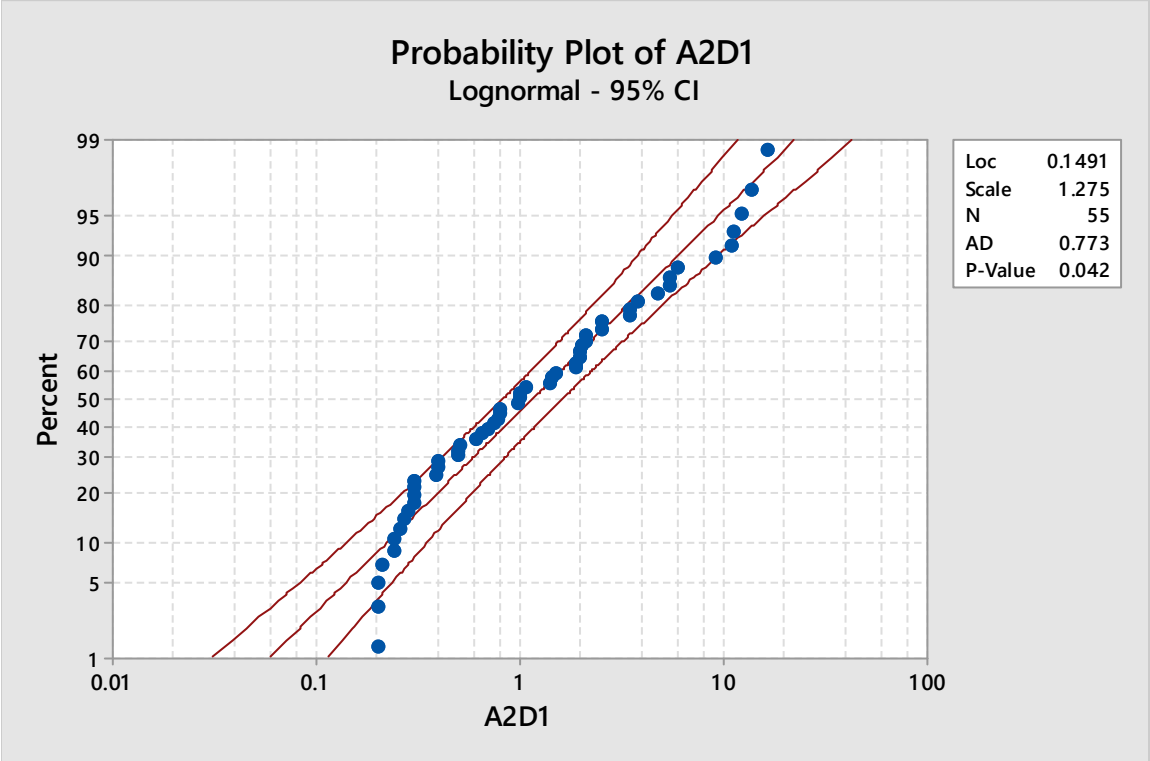

Figure B-7. Lognormal probability plot of A2D1 lithofacies permeability values. The curved lines present 95% confidence intervals.

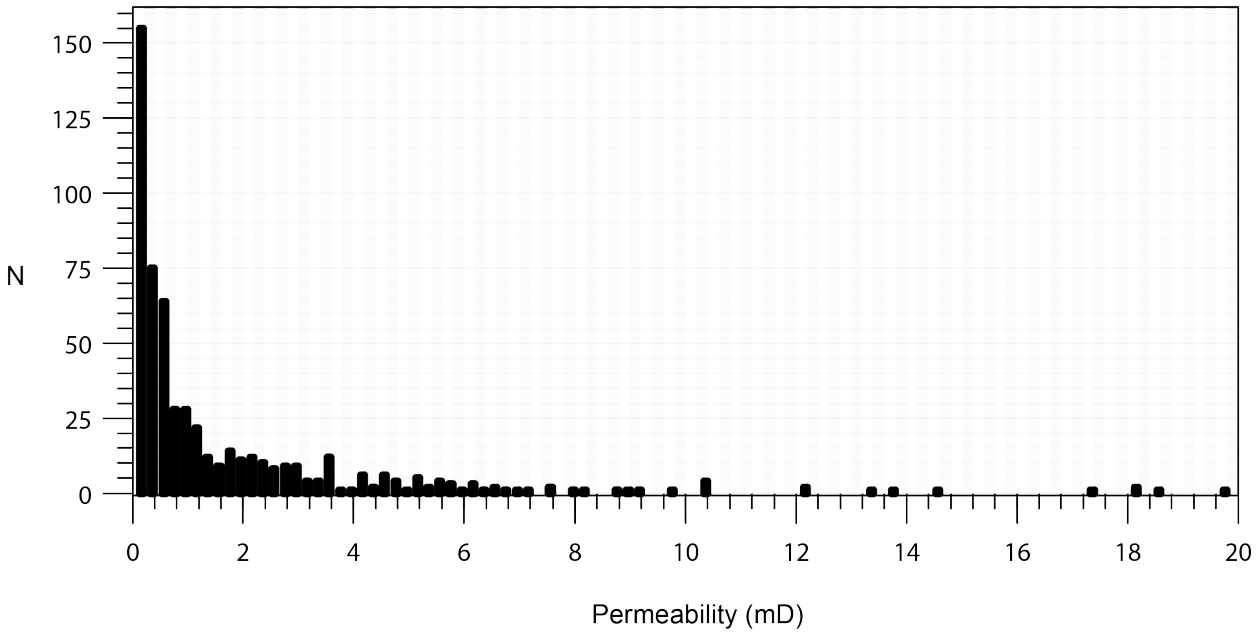

Figure B-8. Histogram of the permeability values measured from core analysis taken in the A2D2 lithofacies in the Overisel field.

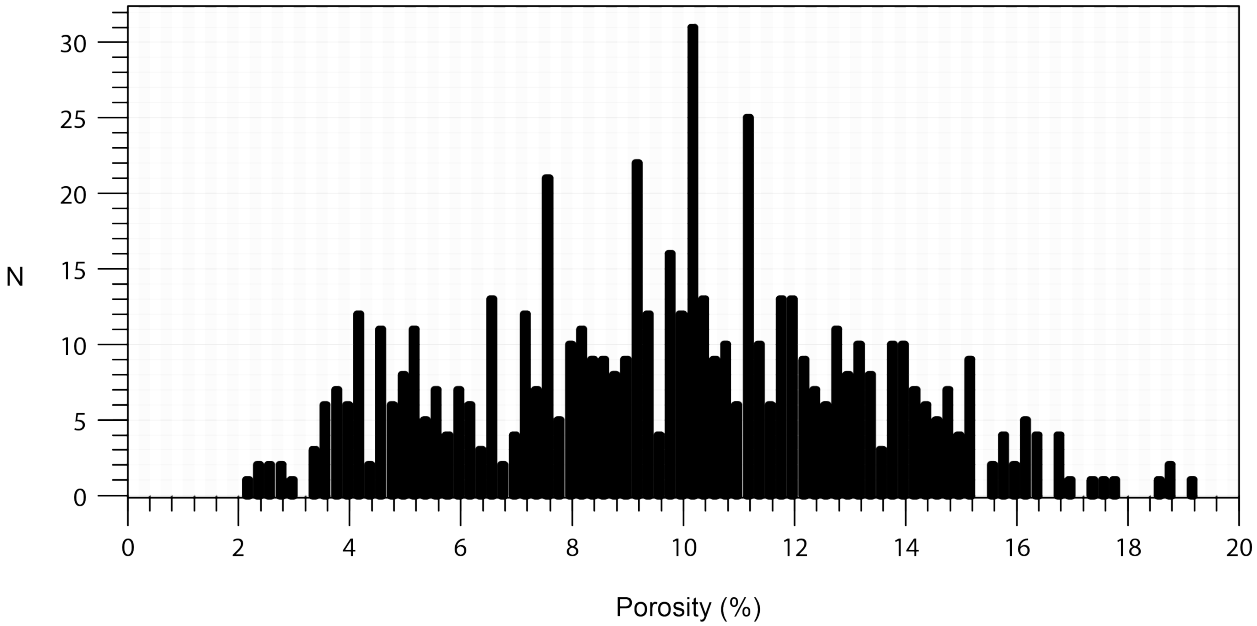

Figure B-9. Histogram of the porosity values measured from core analysis taken in the A2D2 lithofacies in the Overisel field.

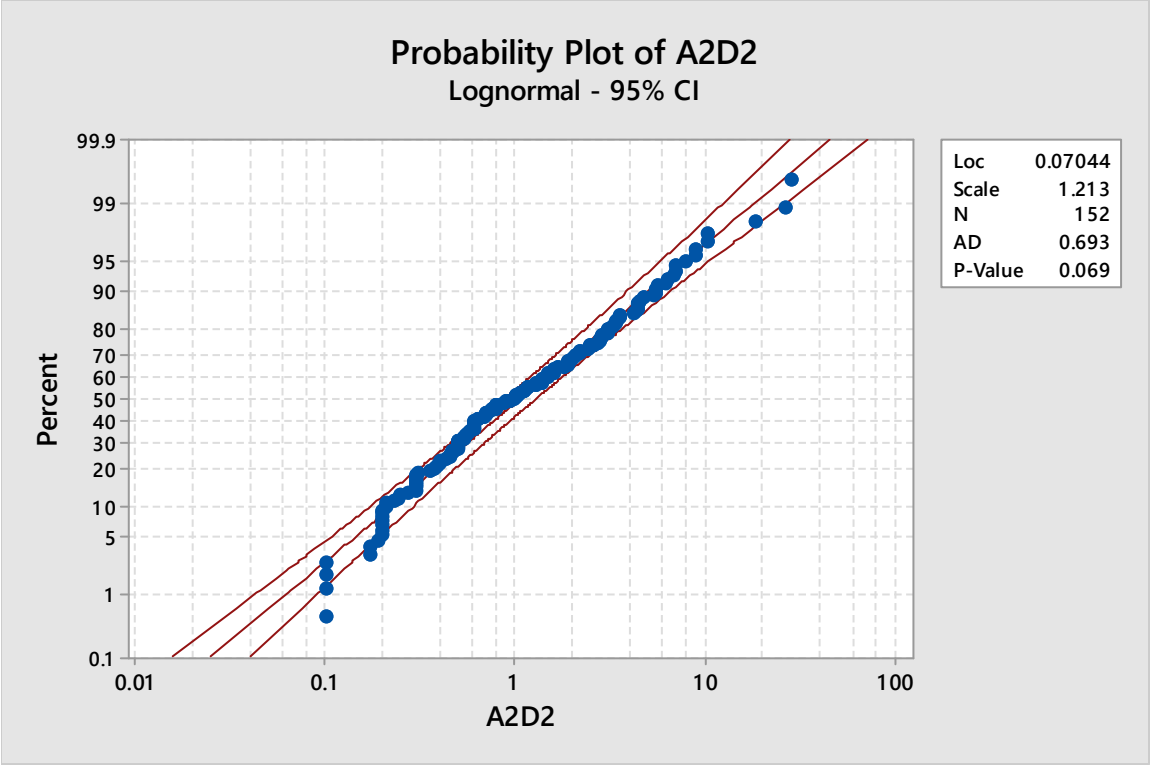

Figure B-10. Lognormal probability plot of A2D2 lithofacies permeability values. The curved lines present 95% confidence intervals.

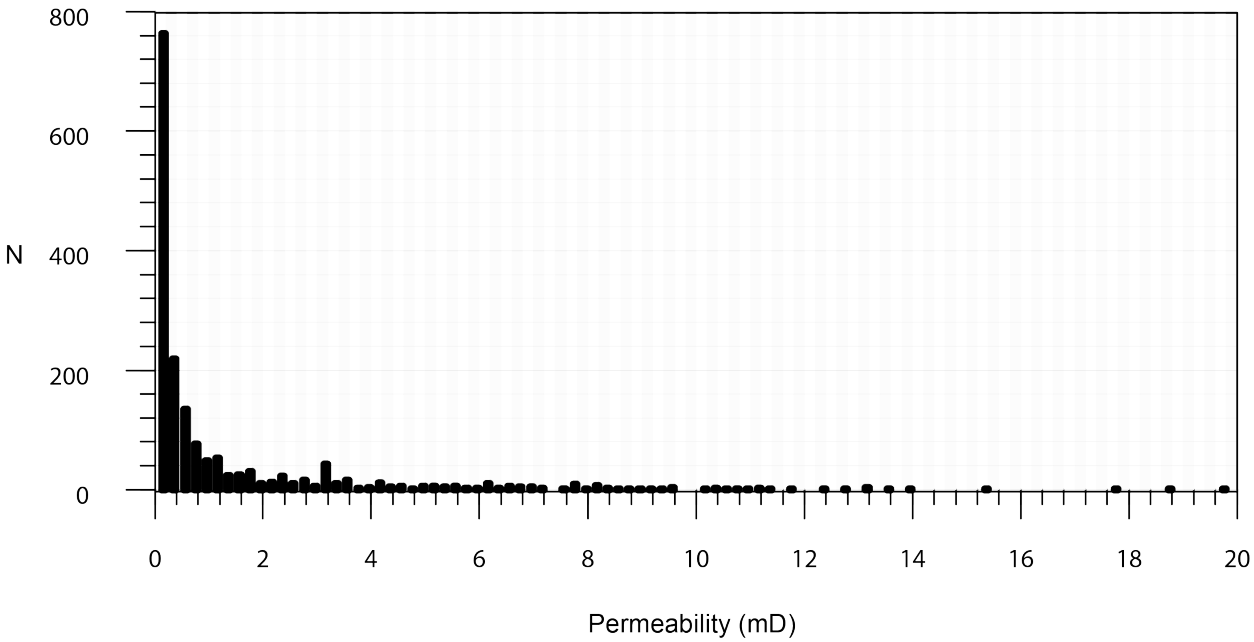

Figure B-11. Histogram of the permeability values measured from core analysis taken in the A2D3 lithofacies in the Overisel field.

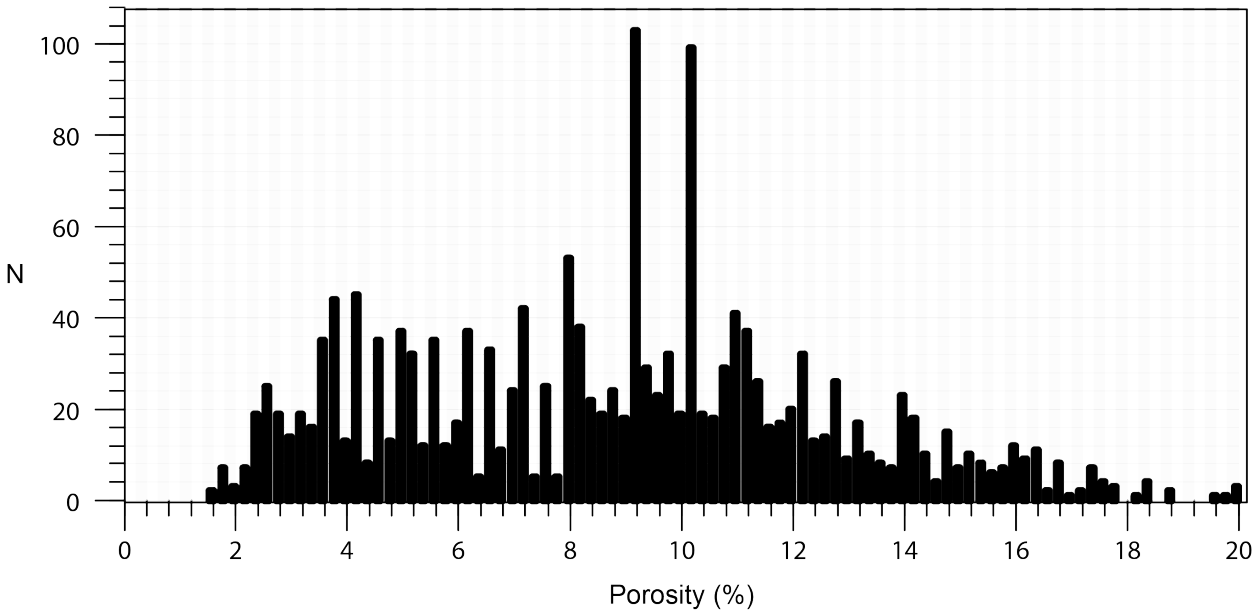

Figure B-12. Histogram of the porosity values measured from core analysis taken in the A2D3 lithofacies in the Overisel field.

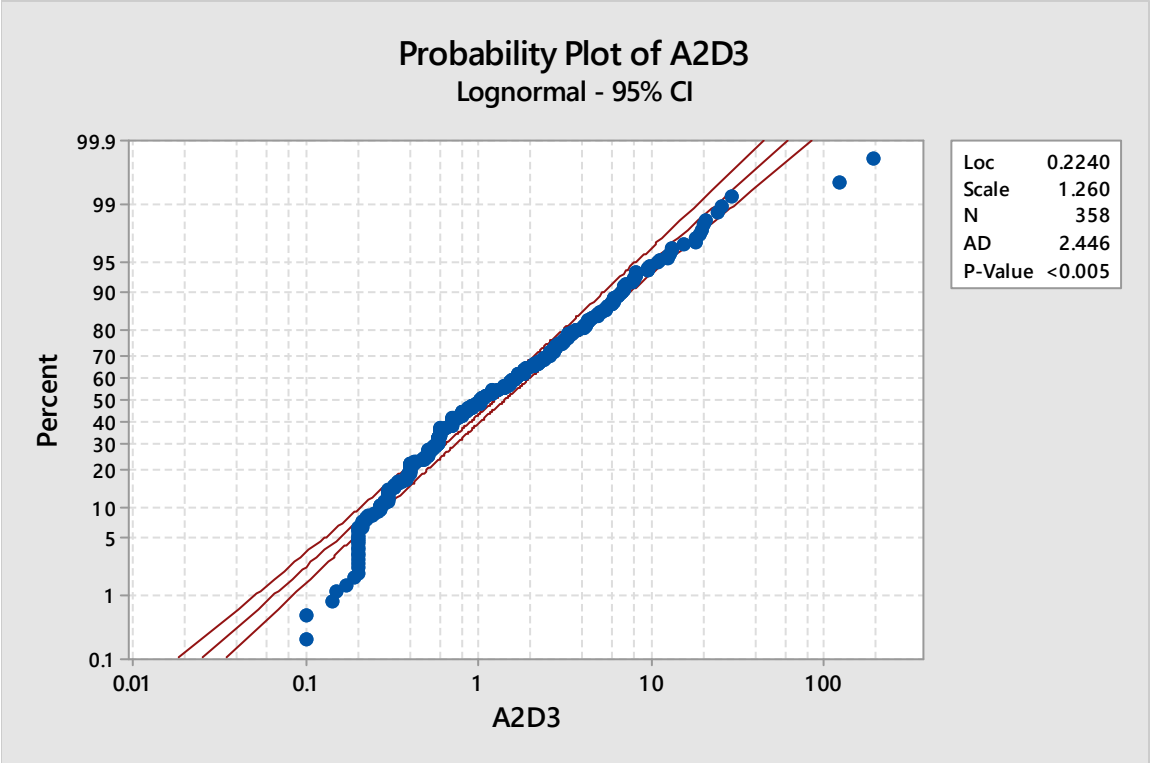

Figure B-13. Lognormal probability plot of A2D3 lithofacies permeability values. The curved lines present 95% confidence intervals.

REFERENCES

Budros, R., and Briggs, L. I. 1977. Depositional Environment of Ruff formation (Upper Silurian) in Southeastern Michigan. *AAPG Studies in Geology: Reefs and Evaporites—Concepts and Depositional Models* **5***:* 53-71.

Butler, G. P. 1969. Modern Evaporite Deposition and Geochemistry of Coexisting Brines, The Sabkha, Trucial Coast, Arabian Gulf. *Journal of Sedimentary Research*, **39**(1): 70-89. https://doi.org/10.1306/74D71BE5-2B21-11D7-8648000102C1865D

Catacosinos, P.A., Daniels, P.A., Harrison, W.B. III, 1991, Structure, Stratigraphy and Petroleum Geology of the Michigan Basin. Amer. Assoc. *Petrol. Geol. Petroleum Basins Series: Interior Cratonic Basins* **Chapter 30**: 561-601.

Cohee, G. V. 1965. Geologic history of the Michigan Basin. *Journal of the Washington Academy of Sciences* **55**(9): 211-223

Cramer, B. D., Brett, C. E., Melchin, M. J., Maennik, P., Kleffner, M. A., McLaughlin, P. I., and Brunton, F. R. 2011. Revised Correlation of Silurian Provincial Series of North America with global and regional chronostratigraphic units and δ13Ccarb chemostratigraphy. *Lethaia*, **44**(2): 185-202.

Dunham, R. J. 1962. Classification of Carbonate Rocks According to Depositional Textures. *AAPG Memoir: Classification of Carbonate Rocks—A Symposium,* **1:** 108-121

Ells, G. D. 1958. Notes on the Devonian-Silurian in the subsurface of southwest Michigan. *State of Michigan, Michigan Geological Survey Progress Report*. **18**: 55

Ells, G. D. 1967. Michigan's Silurian oil and gas pools. *Michigan Geological Survey Report of Investigation*. **2**: 49

Gardner, W. C. 1974. Middle Devonian stratigraphy and depositional environments in the Michigan Basin. *Michigan Basin Geological Society Special Publication*. **1**: 138

Gill, D. 1973. *Stratigraphy, facies, evolution and diagenesis of productive Niagara Guelph reefs and Cayugan sebkha deposits, the River Mills gas field, Michigan Basin.* Doctoral Dissertation, University of Michigan, Ann Arbor, Michigan (1973).

Howell, P. D., and van der Pluijm, B. A. 1999. Structural sequences and styles of subsidence in the Michigan basin. *Geological Society of America Bulletin* **111**(7): 974-991.

Huh, J. M., Briggs, L. I., and Gill, D. 1977. Depositional environments of pinnacle reefs, Niagara and Salina Groups, northern shelf, Michigan Basin. *American Association of Petroleum Geology* **5**: 1-21

Leibold III, A. W. 1992. *Sedimentological and geochemical constraints on Niagara/Salina deposition, Michigan Basin.* Doctoral Dissertation, University of Michigan, Ann Arbor, Michigan (1992).

Lilienthal, R. T. 1974. Subsurface Geology of Barry County. *Michigan: Michigan Department of Natural Resources Report of Investigation* **15**: 1-18.

Matthews, C. S., and Russell, D. G. 1967. *SPE Pressure buildup and flow tests in wells* **1**: 62-66.

McKerrow, W. S., and Scotese, C. R. (Eds.). 1990. Palaeozoic palaeogeography and biogeography. *London: Geological Society*. **12**: 1-21.

Mesolella, K. J., Robinson, J. D., McCormick, L. M., and Ormiston, A. R. 1974. Cyclic deposition of Silurian carbonates and evaporites in Michigan Basin. *AAPG Bulletin*. **58**(1): 34-62.

Pettersen, O., 2006. Basics of Reservoir Simulation. *Lecture Notes*, Department of Mathematics, University of Bergen, Bergen, Norway.

Pyrcz, M. and C. Deutsch. 2014. Geostatistical Reservoir Modeling, *Oxford University Press.*: 429.

Rine, M. J. 2015. Depositional Facies and Sequence Stratigraphy of Niagaran-Lower Salina Reef Complex Reservoirs of the Guelph Formation, Michigan Basin. Master's Thesis, Western Michigan University, Kalamazoo, Michigan (2015).

Rivenaes, j., Sorhaug P., and Knarud R. 2015. Introduction to Reservoir Modeling in Petroleum Geoscience. *Sedimentary Environments to Rock Physics* **2**: 559-580.

Schlumberger PETREL. 2015. E&P Software Platform, *user manual*, **2015** (1).

Society of Petroleum Engineers (SPE). 2015. Natural Gas Properties. *PetroWiki,* 24 June 2015, https://petrowiki.org/Natural_gas_properties#cite_note-r2-2 (accessed October 2018).

Society of Petroleum Engineers (SPE). 2015. Gas Well Deliverability. *PetroWiki*, 12 June 2015, https://petrowiki.org/Gas_well_deliverabilityttp (accessed October 2018).

Society of Petroleum Engineers (SPE). 2015. Gas Formation Volume Factor and Density. *PetroWiki*, 9 July 2015, https://petrowiki.org/Gas_formation_volume_factor_and_density (accessed October 2018).

State of Michigan. 2018a. GeoWebFace. *Department of Environmental Quality*, 2018, http://www.deq.state.mi.us/GeoWebface/ (accessed September 2018).

State of Michigan. 2018b. Michigan Natural Gas Storage Field Summary. *Department of Licensing and Regulatory Affairs*, 2018 https://www.michigan.gov/mpsc/0,4639,7-159-16385_59482-426107--,00.html#tab=Active (accessed February 2018).

Stein, C. A., Stein, S., Elling, R., Keller, G. R., and Kley, J. 2018. Is the "Grenville Front" in the central United States really the Midcontinent Rift? *GSA Today* **28**(5): 4-10.

Tremper, L. R. 1973. Lithofacies and stratigraphic analysis of the Salina group of the" North Slope" of the Michigan Basin. Doctoral Dissertation, University of Michigan, Ann Arbor, Michigan (1973).

US Department of Energy. 2016. U.S. Energy Information Administration – EIA – Independent Statistics and Analysis. *U.S. States – Ranking – U.S. energy Information Administration (EIA)*, 2016, www.eia.gov/state/rankings/. (accessed February 2018).

Wright, V.P. 1984. Peritidal carbonate facies models: A review. *Geological Journal* **19**: 309-325.